

# Diagnostic Imaging for Retinoblastoma Cancer Staging: Guide for Providing Essential Insights for Ophthalmologists and Oncologists

Vivek Pai, MBBS, MD • Prakash Muthusami, MBBS, MD • Birgit Ertl-Wagner, MD, PhD, MHBA • Manohar M. Shroff, MD, DMRD  
Carmen Parra-Fariñas, MD, PhD • Kanchan Sainani, MBBS, MS • Stephanie Kletke, MD • Marie-Anne Brundler, MD • Ashwin Mallapatna, MBBS, MD

Author affiliations, funding, and conflicts of interest are listed at [the end of this article](#).



Retinoblastoma is the most common cause of all intraocular pediatric malignancies. It is caused by the loss of *RBI* tumor suppressor gene function, although some tumors occur due to *MYCN* oncogene amplification with normal *RBI* genes. Nearly half of all retinoblastomas occur due to a hereditary germline *RBI* pathogenic variant, most of which manifest with bilateral tumors. This germline *RBI* mutation also predisposes to intracranial midline embryonal tumors. Accurate staging of retinoblastoma is crucial in providing optimal vision-, eye-, and life-saving treatment. The *AJCC Cancer Staging Manual* has undergone significant changes, resulting in a universally accepted system with a multidisciplinary approach for managing retinoblastoma. The authors discuss the role of MRI and other diagnostic imaging techniques in the pretreatment assessment and staging of retinoblastoma. A thorough overview of the prevailing imaging standards and evidence-based perspectives on the benefits and drawbacks of these techniques is provided.

Published under a CC BY 4.0 license.



Test Your Knowledge

RadioGraphics 2024; 44(4):e230125  
<https://doi.org/10.1148/rg.230125>

Content Codes: NR, PD

Abbreviations: AJCC = American Joint Committee on Cancer, OCT = optical coherence tomography, ON = optic nerve, 3D = three dimensional

## TEACHING POINTS

- Histopathologic high-risk features for metastasis and posttreatment recurrence include massive choroidal invasion, postlaminar ON invasion, anterior segment involvement, and scleral and extrascleral invasion.
- Caution must be exercised because the absence of vitreous seeding at MRI does not rule out its presence.
- Discontinuity and thickening of the normal curvilinear choroid may be an imaging marker of choroid invasion. Accurate detection of choroid invasion at MRI is often hampered by the extent of retinal destruction.
- Abnormal anterior chamber enhancement in patients with retinoblastoma must alert the radiologist and ophthalmologist to the aggressive behavior of the tumor and to the possibility of high-risk features.
- In contradistinction to prelaminar ON involvement, postlaminar ON invasion has been identified as a high-risk feature for poor prognosis with increased risk of orbital recurrence after enucleation.

## Introduction

Retinoblastoma is the most common pediatric primary intraocular tumor, accounting for 4% of all pediatric malignancies (1,2). Its incidence varies between one in 16 000 and one in 18 000 live births, annually contributing about 8000 new cases worldwide (3,4). There are no geographic or racial predilections; populations with high birth rates have a higher disease burden (4).

The *RBI* gene is a tumor suppressor gene on the long arm of chromosome 13 (13q14) (5). Almost all retinoblastomas are caused by complementary biallelic mutations of *RBI* (Knudson “2-hit” hypothesis). Approximately 60% of cases are sporadic, where somatic mutations occur in a retinal progenitor cell resulting in a unilateral tumor (5). The rest carry a germline variant in *RBI*, inherited in an autosomal dominant manner (5). More than 90% of patients with the germline variant develop retinoblastoma; others remain unaffected carriers (1,5). In the heritable form, the first is a germline mutation present in every cell of an individual, and the second somatic mutation occurs in retinal progenitor cells of both eyes, thus often causing bilateral and/or multifocal retinoblastomas (5).

Few patients (<6%) may have a deleted *RBI* gene with contiguous parts of the 13q14 gene locus, termed 13q deletion syndrome. These children can also demonstrate facial dysmorphism (anteverted pinnae, broad forehead, short nose, prominent philtrum, thick lower lip) (5). Less than 3% of patients with unilateral lesions below the age of 12 months develop retinoblastoma with *MYCN* oncogene amplification without a detectable *RBI* mutation (5). These tumors are clinically similar to those in patients with the *RBI* mutation but are not associated with familial transmission and do not predispose to development of secondary malignancies (5).

In high-income countries, retinoblastoma is diagnosed by the age of 3 years in 80% of patients and by the age of 5 years in 95% of patients (1). Bilateral retinoblastomas are typically diagnosed around 15 months of age and unilateral tumors



**Figure 1.** Clinical photograph shows leukokoria in a 6-month-old boy with retinoblastoma.

around 24 months of age (5). Leukokoria is the most common presenting sign (22.6%–97.9%) and occurs due to light reflecting off the retinoblastoma or its seeds (Fig 1) (2). Strabismus may be secondary to diminished vision from macular involvement or retinal detachment (2). Patients with advanced tumors may present with proptosis and ecchymosis (2).

Generally, retinoblastomas are creamy white encephaloid lesions with chalky calcification and yellowish necrosis, originating from the inner nuclear layer of the retina (6,7). Endophytic tumors affect the inner retinal layers and invade the vitreous, while exophytic tumors affect the outer retinal layers and grow outward. The majority of tumors show a combination of both growth patterns (1). Diffuse anterior retinoblastoma is an uncommon plaquelike endophytic tumor encountered in older children (5–12 years of age) (8). These arise from the retinal periphery and involve ocular structures anterior to the anterior vitreous margin (anterior vitreous face) such as the pars plicata, lens zonules, and iris (8).

At histopathologic analysis, retinoblastomas are composed of small hyperchromatic cells with a high nuclear-to-cytoplasmic ratio (6). Calcifications and necrosis are common (6). Tumor cells may be arranged in a spoke-wheel pattern around a central core, known as rosettes, with Flexner-Wintersteiner rosettes (cuboidal cells surrounding a central lumen) and Homer Wright rosettes (tumor cells surrounding a tangle of neural filaments) being pathognomonic (9) (Figs 2, 3). Histopathologic high-risk features for metastasis and posttreatment recurrence include massive choroidal invasion, postlaminar optic nerve (ON) invasion, anterior segment involvement, and scleral and extrascleral invasion (6).

Multiple systems of classification and staging have been used. Proposed in the 1960s, the Reese-Ellsworth classification grouped intraocular retinoblastomas on the basis of clinical features that impact outcomes of external beam radiation therapy (10). With the advent of chemotherapy and

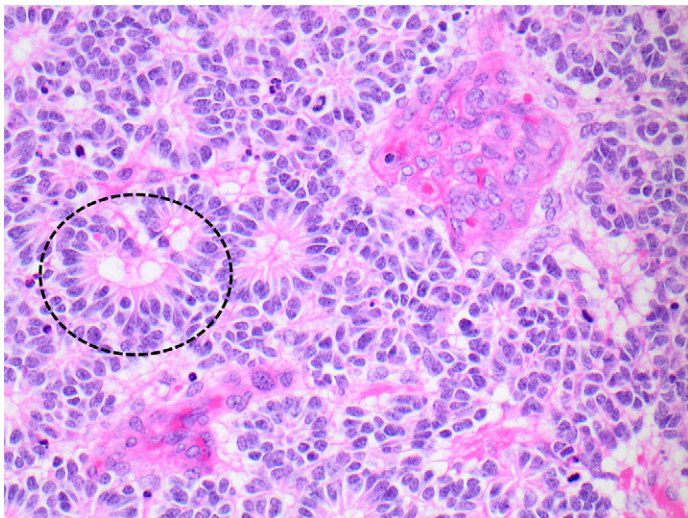


**Figure 2.** High-power magnification of a histopathologic specimen from a patient with retinoblastoma shows areas of undifferentiated blue tumor cells, with some areas showing a characteristic differentiation into Flexner-Wintersteiner rosettes (oval) with an empty lumen.

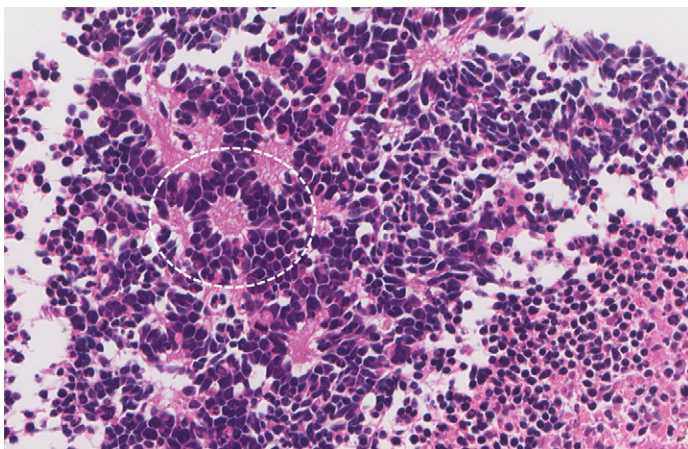


**Figure 3.** High-power magnification of a histopathologic specimen shows Homer Wright rosettes (oval) with basophilic cells and a central core of primitive neuronal processes (neuropil).

focal consolidation, two superficially similar but significantly varied consensus-based classification systems emerged—the International Intraocular Retinoblastoma Classification (IIRC) and the International Classification of Retinoblastoma (ICRB). These used the same group names (A–E) with different definitions, hindering collation of evidence needed to predict treatment outcomes (11). The eighth edition of the American Joint Committee on Cancer (AJCC) staging guidelines defines anatomic locations and stages of tumor growth (T) with regional nodal (N) and systemic metastasis (M), as well as heritability (H) as an independent category (11,12) (Table 1). It also includes pathologic staging for enucleated eyes (Table 2) (12).

In this article, we discuss the role and limitations of MRI and other diagnostic imaging modalities in the evaluation of the various clinical AJCC stages of retinoblastoma. A comprehensive evidence-based review of the advantages and limitations of MRI on the pretreatment evaluation of retinoblastoma is also provided.

**Table 1. AJCC Clinical Retinoblastoma Staging (cTNMH)**

| Stage | Description  |
|-------|--|
| cT1   | Intraocular tumor(s) with subretinal fluid $\leq 5$ mm from base of any tumor  |
| cT1a  | Tumors $\leq 3$ mm and further than 1.5 mm from disc and fovea   |
| cT1b  | Tumors $>3$ mm or closer than 1.5 mm from disc or fovea  |
| cT2   | Intraocular tumor(s) with retinal detachment, vitreous seeding, or subretinal seeding  |
| cT2a  | Subretinal fluid $>5$ mm from the base of any tumor  |
| cT2b  | Vitreous seeding and/or subretinal seeding   |
| cT3   | Advanced intraocular tumor(s)  |
| cT3a  | Phthisis or prephthisis bulbi  |
| cT3b  | Tumor invasion of choroid, pars plana, ciliary body, lens, zonules, iris, or anterior chamber  |
| cT3c  | Raised intraocular pressure with neovascularization and/or buphthalmos   |
| cT3d  | HypHEMA and/or massive vitreous hemorrhage   |
| cT3e  | Aseptic orbital cellulitis   |
| cT4   | Extraocular tumor(s) involving orbit, including the ON   |
| cT4a  | Radiologic evidence of retrobulbar ON involvement or thickening of the ON or involvement of orbital tissues  |
| cT4b  | Extraocular tumor clinically evident with proptosis and/or an orbital mass   |
| N1    | Evidence of preauricular, submandibular, and cervical lymph node involvement   |
| cM1   | Clinical signs of distant metastasis   |
| cM1a  | Tumor(s) involving any distant site (eg, bone marrow, liver) at clinical examination or radiologic imaging   |
| cM1b  | Tumor involving the central nervous system at radiologic imaging (not including trilateral retinoblastoma)   |
| H     | Hereditary trait   |
| HX    | Unknown or insufficient evidence of a constitutional <i>RBI</i> gene mutation  |
| H0    | Normal <i>RBI</i> alleles in blood tested with demonstrated high-sensitivity assays<br>H0* is assigned if the possibility of very low-level mosaicism cannot be ruled out  |
| H1    | Bilateral retinoblastoma, retinoblastoma with an intracranial primitive neuroectodermal tumor (ie, trilateral retinoblastoma), patient with family history of retinoblastoma, or molecular definition of a constitutional <i>RBI</i> gene mutation |

Source.—Reference 12.

## Diagnostic Workup: Ophthalmology

### Wide-Field Fundus Photography and Fluorescein Angiography

An examination of both eyes under anesthesia is crucial for staging and management (13). Traditionally, retinal drawings pictorially described lesion topography. Digital wide-field images are now obtained with a hand-held fundus camera, such

**Table 2: AJCC Pathologic Staging (pTNM)**

| Stage | Description   |
|-------|---|
| pT1   | Intraocular tumor(s) without any local invasion, or with focal choroidal invasion, or pre- or intralaminar involvement of the ON head   |
| pT2   | Intraocular tumor(s) with local invasion  |
| pT2a  | Intraocular tumor(s) with focal choroidal invasion and pre- or intralaminar involvement of the ON head  |
| pT2b  | Tumor invasion of stroma of iris and/or trabecular meshwork and/or Schlemm canal  |
| pT3   | Intraocular tumor(s) with significant local invasion  |
| pT3a  | Massive choroidal invasion (>3 mm in largest diameter, or multiple foci of focal choroidal involvement totaling >3 mm, or any full-thickness choroidal involvement)   |
| pT3b  | Retrolaminar invasion of the ON head, not involving the transected end of the ON  |
| pT3c  | Any partial-thickness involvement of the sclera within the inner two-thirds   |
| pT3d  | Full-thickness invasion into the outer third of the sclera and/or invasion into or around emissary channels   |
| pT4   | Extraocular tumor(s) involving orbit, including the ON<br>Evidence of extraocular tumor: tumor at the transected end of the ON; tumor in the meningeal spaces around the ON; full-thickness invasion of the sclera with invasion of the episclera, adjacent adipose tissue, extraocular muscle, bone, conjunctiva, or eyelids |

Source.—Reference 12.

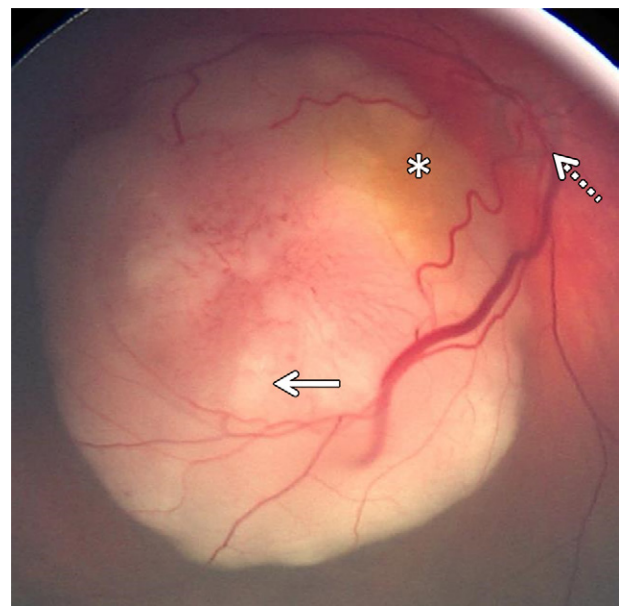


**Figure 4.** Wide-field fundus image shows a solitary creamy-white retinoblastoma, with focal bright white spots corresponding to areas of dystrophic calcification (solid arrow). The tumor occupies the posterior pole of the right eye, temporal to the optic disc (dotted arrow). The yellow xanthophyll pigment noted in the superonasal edge of the tumor indicates the fovea centralis (\*), the retinal locus important for central vision and visual acuity.

as the RetCam (Clarity Medical), which captures high-resolution retinal, vitreal, and anterior segment images (Fig 4) (13).

Fluorescein angiography is an imaging technique that uses sodium fluorescein, a water-soluble dye, administered intravenously (3). The dye fluoresces when excited by blue light (465–490 nm), emitting light in the green spectrum (520–530 nm) (3). This delineates retinal vascular changes due to the tumor and helps assess posttreatment changes (3).

**Optical Coherence Tomography**

Optical coherence tomography (OCT) is a noninvasive light interference–based imaging modality used to obtain high-resolution (<10 μm) cross-sectional images of the retina (14). On OCT images, small retinoblastomas are isorefective with smooth margins, originating from the inner nuclear layer (Fig 5) (15,16). Larger lesions grow to occupy the outer and middle retinal layers, obscuring underlying structures (15,16). OCT is also used in monitoring treatment response and detection of tumor recurrences (15). Phase-based OCT angiography uses changes in the phase of OCT signals (Doppler effect) caused by mobile blood cells, thus differentiating vessels from static tissues and eliminating the need for contrast material administration (3,17).

**Ultrasonography**

US uses a 10–20-MHz high-frequency probe to achieve a resolution of 150 microns (3). At B-mode US, retinoblastomas are heterogeneous hyperechoic intraocular masses with cal-

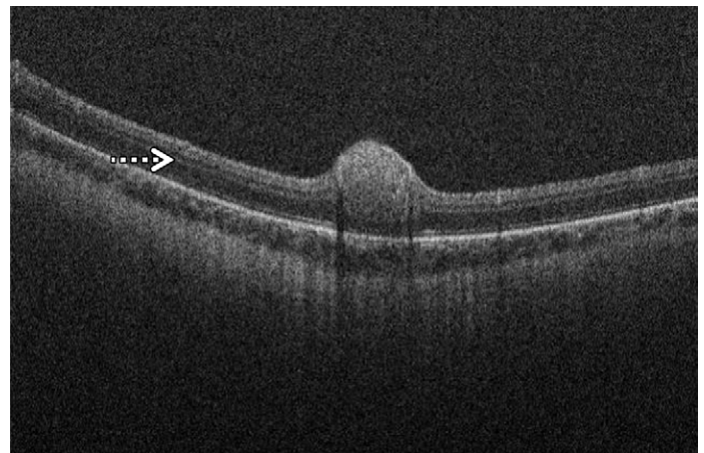


**Figure 5.** Optical-coherence tomographic image shows a small intraretinal retinoblastoma originating from the inner nuclear layer (arrow) of the retina and disrupting the normal retinal lamination.

cifications causing acoustic shadowing (Fig 6) (12). Retrobulbar imaging may allow evaluation of ON invasion (12). Color Doppler imaging has shown significant correlation between tumor volume and resistivity indices of the central retinal artery with ON invasion, correlating with reduced central retinal vein pulse index (18). Advances in transducer technology allow acquisition of three-dimensional (3D) images and hence provide better delineation of high-risk features (19). A US biomicroscope uses high-frequency transducers (50 MHz) to provide in vivo analysis of the anterior segment of the eyeball at a high resolution (30–50 microns) (3,12).

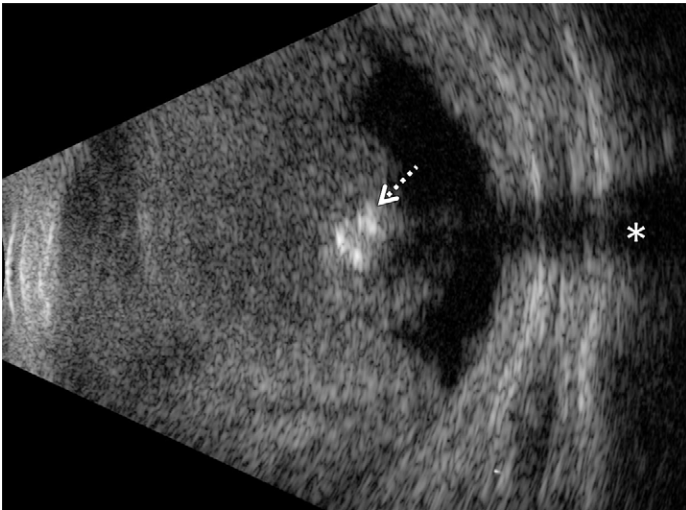


**Figure 6.** B-mode US of retinoblastoma. Axial US image in a 26-month old girl shows an echogenic retinoblastoma occupying the vitreous chamber, with foci of intralesional calcification (arrow) causing posterior acoustic shadowing (\*).

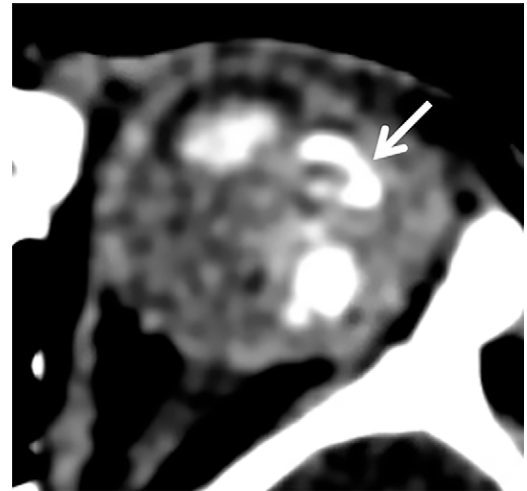


**Figure 7.** Retinoblastoma in a 14-month-old boy who presented with leukokoria. Axial CT image obtained by using a brain parenchymal kernel shows a large hyperattenuating retinoblastoma (arrow) with foci of calcifications within.

## Diagnostic Workup: Radiology

### Computed Tomography

Retinoblastomas are hyperattenuating compared with the vitreous and demonstrate moderate contrast enhancement (Fig 7) (20). Most retinoblastomas (85%–95%) have calcifications, a feature differentiating them from clinical mimics (21,22). CT has a sensitivity of 81%–96% in detecting retinoblastoma calcifications (22). However, the sensitivity of CT for detection of ON invasion is low, even in cases of extensive involvement (20). The use of CT in retinoblastoma workup has steadily declined due to the theoretical risk of developing secondary malignancies from ionizing radiation in CT, along with the contemporaneous advancements in MRI (1).

### MRI: Tumor Characteristics

MRI provides excellent contrast resolution, making it the radiologic modality of choice for evaluating retinoblastoma (22). Retinoblastomas are mildly hyperintense on T1-weighted images and hypointense on T2-weighted images (relative to vitreous) (23). On T2\* images, intralesional calcifications show signal void T2\* signals. In vivo signal voids in retinoblastoma on T2\*-weighted images correlate well with calcification on ex vivo CT images (21). Hemorrhage, often associated with necrotic lesions, may mimic calcification (21). Peripheral linear areas of low T2\* signal intensity suggest intratumoral hemorrhage, while calcifications are usually central and nodular (21). Retinoblastomas usually demonstrate restricted diffusion and heterogeneous contrast enhancement (Fig 8) (23,24). Necrotic tumor components may not demonstrate enhancement (24).

A summary of the suggested MRI guidelines by the European Retinoblastoma Imaging Collaboration (Table 3) and our institutional protocols (Table 4) are provided.

### MRI: Imaging Features Impacting AJCC Staging

MRI plays a crucial role in the preoperative evaluation of retinoblastoma. While it helps in confirming the clinical diagnosis, it also enables assessment of tumor invasion of the choroid, sclera, and ON, all of which are high-risk features for systemic dissemination. Additionally, it helps identify concomitant intracranial metastasis and embryonal tumors (25). These factors impact treatment planning and prognosis.

### Tumor Size and Relation with Optic Disc and Fovea

Retinoblastomas smaller than 3 mm at the base and 2 mm in thickness can be treated with focal lasers or cryotherapy alone. Larger lesions require longer or multiple focal therapy sessions causing ocular complications and partial tumor control (26–28). In fact, lesions occupying more than two-thirds of the globe volume are associated with a 2.6-fold increased risk of harboring high-risk features (29). Such lesions may need chemotherapy followed by laser consolidation (27,28,30). For discrete lesions, estimation of the distance of the tumor from the fovea is critical, as close foveal proximity increases the risk of visual loss from the tumor or laser-related damage (27,28,30).

Retinal examination and OCT are more sensitive than MRI in the detection of small tumors (31). While moderate to large tumors are readily identifiable on MR images, small lesions may be detected with heavily T2-weighted high-spatial-resolution 3D imaging techniques (Fig 9) (20). These sequences can be used to estimate the foveal location as well; that is, 16° temporal to the optic disc (31).

The disc is the site where retinal ganglion cells converge (prelaminar ON) and traverse a reticulated structure at the scleral foramen, known as the lamina cribrosa, to form the postlaminar ON (32). At MRI, the disc is located at the level of the normal posterior discontinuity of the sclera; that is, at the ON insertion (3). The lamina cribrosa is located at the junction

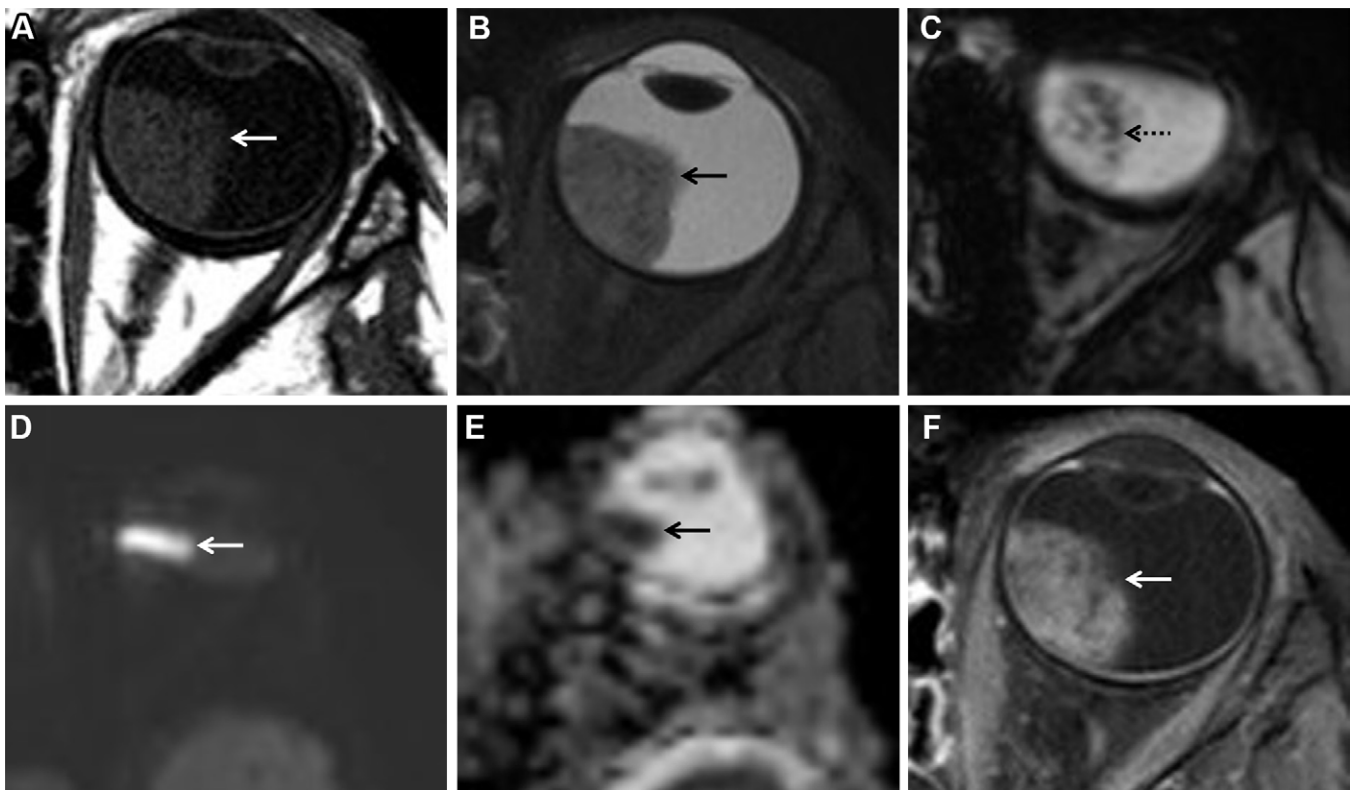


**Figure 8.** General MRI appearance of retinoblastoma in a 4-year-old girl. **(A)** Axial T1-weighted image shows a lobulated retinoblastoma (arrow) within the left globe with mildly hyperintense signal relative to that of the vitreous. **(B)** Axial fat-saturated T2-weighted image shows hypointense signal within the retinoblastoma (arrow) relative to that of the vitreous. **(C)** Axial gradient-echo MR image shows foci of blooming (arrow) within the retinoblastoma corresponding to areas of calcification. **(D, E)** Axial diffusion-weighted (*b* value = 1000 mm<sup>2</sup>/sec) **(D)** and apparent diffusion coefficient **(E)** images show restricted diffusion within the retinoblastoma (arrow). **(F)** Axial contrast-enhanced fat-saturated T1-weighted MR image shows avid nearly homogeneous enhancement within the retinoblastoma (arrow).

**Table 3: Imaging Guidelines from the European Retinoblastoma Imaging Collaboration\***

| Anatomy                    | Sequence                        | Plane                      | Thickness | Comments  |
|----------------------------|---------------------------------|----------------------------|-----------|---|
| Globe                      | T2 weighted                     | Axial                      | ≤2 mm     | Fat saturation not mandatory; image both globes, regardless of laterality |
| Globe                      | 3D steady-state free precession | Axial                      | ≤1 mm     | Optional; small tumors; comparison of eye size and anterior chamber depth |
| ON                         | Precontrast T1 weighted         | Axial and sagittal oblique | ≤2 mm     | Bilateral disease only axial plane would suffice                          |
| ON                         | T2 weighted                     | Axial and sagittal oblique | ≤2 mm     | Bilateral disease only axial plane would suffice                          |
| ON                         | Postcontrast T1 weighted        | Axial and sagittal oblique | ≤2 mm     | Fat saturation not mandatory  |
| Brain (overview)           | T2 weighted                     | Axial                      | ≤4 mm     | Rule out structural abnormalities in 13q deletion syndrome                |
| Brain metastasis           | Postcontrast T1 weighted        | Two-dimensional            | ≤3 mm     | Alternate: 3D gradient echo with section thickness ≤1 mm                  |
| Pineal gland cystic lesion | High-resolution 3D T2 weighted  | Coronal and sagittal       | 1.5 mm    | Optional  |

Note.—Adapted and reprinted under a CC BY-NC 4.0 license from reference 20.

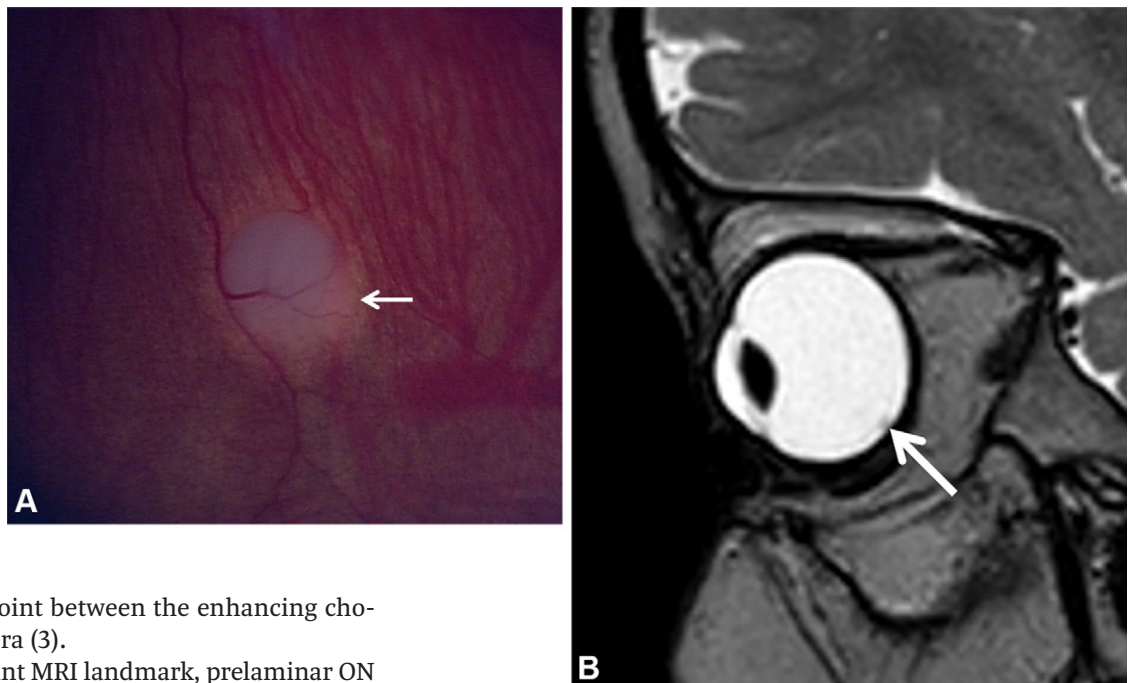
\* General recommendations: MRI under general anesthesia is suggested to ensure optimal patient positioning and achieve complete eye closure and limit ocular movement. Imaging with a 1.5-T system with a head coil does not yield an adequate signal-to-noise ratio. Should a 1.5-T system be used, imaging with surface coils (diameter, ≤5 cm) has been recommended. On a 3-T system, a multichannel head coil or surface coils may be used.

**Table 4: Institutional Protocol at the Hospital for Sick Children for Imaging the Orbits in Patients with Retinoblastoma**

| Sequence                                | Plane            | Fat Saturation | Section Thickness       | TR (msec)             | TE (msec) | Flip Angle (°) | Matrix    | Time (min:sec) |
|---|------------------|----------------|-------------------------|-----------------------|-----------|----------------|-----------|----------------|
| <b>Orbits</b>                           |                  |                |                         |                       |           |                |           |                |
| T1 weighted                             | Axial            | No             | 2 mm                    | 545                   | 19        | 90             | 268 × 265 | 3:39           |
| T2 weighted                             | Axial            | Yes            | 2 mm                    | 3679                  | 81        | 90             | 300 × 300 | 4:32           |
| T2 weighted                             | Coronal          | Yes            | 2 mm                    | 5421                  | 63        | 90             | 280 × 270 | 3:15           |
| T2 weighted                             | Oblique sagittal | Yes            | 2 mm                    | 3000                  | 66        | 90             | 244 × 235 | 4:36           |
| Contrast-enhanced T1 weighted           | Axial            | Yes            | 2 mm                    | 554                   | 20        | 90             | 268 × 265 | 3:43           |
| Contrast-enhanced T1 weighted           | Coronal          | Yes            | 2 mm                    | 630                   | 19        | 90             | 268 × 266 | 2:21           |
| Contrast-enhanced T1 weighted           | Oblique sagittal | Yes            | 2 mm                    | 589                   | 21        | 90             | 268 × 264 | 3:46           |
| <b>Brain</b>                            |                  |                |                         |                       |           |                |           |                |
| Diffusion-weighted imaging              | Axial            | NA             | 3 mm                    | 5972                  | 84        | 90             | 168 × 114 | 2:05           |
| Multiplanar gradient recalled           | Axial            | NA             | 2.67 mm                 | 1348                  | 16        | 18             | 244 × 199 | 2:16           |
| 3D T1-weighted MPRAGE                   | Sagittal         | No             | 1 × 0.76 × 1 (voxel)    | 4.4                   | 2.1       | 8              | 220 × 220 | 1:11           |
| FLAIR                                   | Axial            | No             | 5 mm                    | 10000 (TR) /2850 (TI) | 150       | None           | 276 × 156 | 2:00           |
| Contrast-enhanced 3D T1-weighted MPRAGE | Axial            | Yes            | 0.9 × 0.9 × 0.9 (voxel) | 7                     | 3.3       | 8              | 312 × 192 | 4:59           |
| Time-of-flight MR angiography           | Axial            | No             | 0.4 × 0.6 × 1 (voxel)   | 25                    | 3.5       | 20             | 352 × 234 | 5:22           |

Note.—MPRAGE = magnetization-prepared rapid gradient echo, NA = not applicable, TE = echo time, TI = inversion time, TR = repetition time.  
 \* All imaging examinations for retinoblastoma evaluation are performed on a 3-T MRI unit using a right-channel head coil with the patient under general anesthesia.

**Figure 9.** Retinoblastoma distal from the optic disc and fovea (cT1a) of the left eye in an 18-month-old boy. **(A)** Magnified fundus image shows a small white intraretinal retinoblastoma (arrow). **(B)** Sagittal reconstruction from a heavily T2-weighted 3D sequence performed in the axial plane shows a corresponding retinoblastoma (arrow) along the inferior retinal periphery, distant from the optic disc (not shown).



between the disc and midpoint between the enhancing choroid and nonenhancing sclera (3).

Although it is an important MRI landmark, prelaminar ON invasion is not associated with an increased metastatic risk (33). Involvement of the prelaminar ON can be suspected at MRI when tumor interrupts the normal linear enhancement of the choroidoretinal complex at the disc. However, its absence does not rule out microscopic invasion (Fig 10) (34). The sensitivity and specificity of MRI in detecting prelaminar ON invasion has been reported as 66% and 96%, respectively, with

an accuracy of 79% (34). A strong association between tumor size and prelaminar ON invasion has been described (34).

**Retinal Detachment**

Exudative retinal detachment is common in exophytic retinoblastomas, usually resolving spontaneously after chemo-

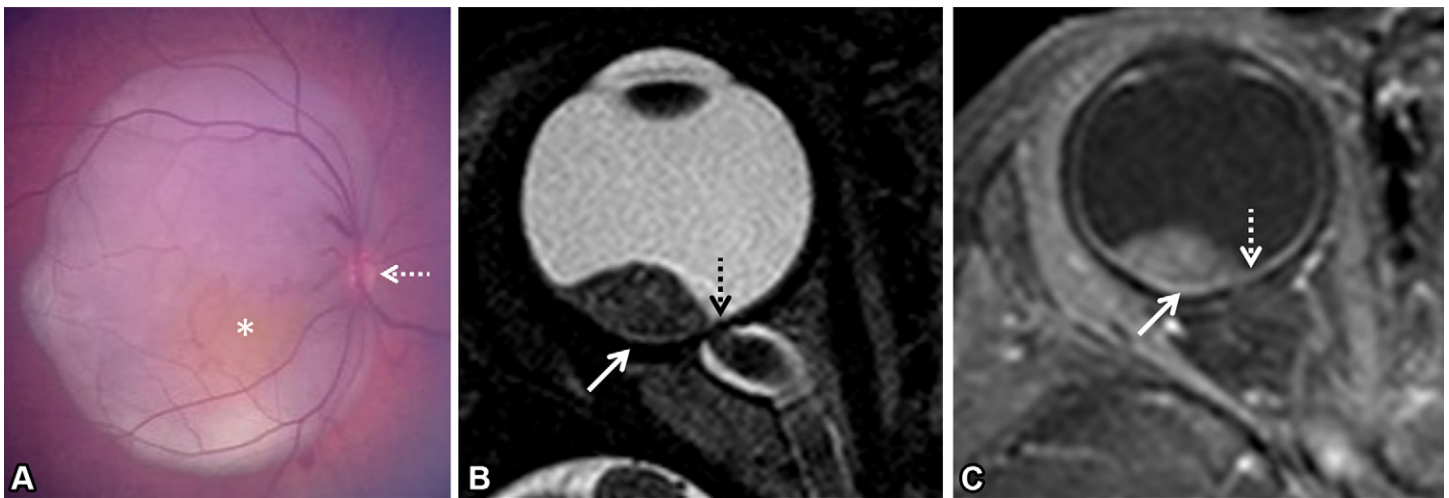


**Figure 10.** Retinoblastoma (stage cT1b) of the right eye in a 3-year-old girl. **(A)** Wide-field retinal image shows a retinoblastoma (>3 mm in greatest dimension) occupying the fovea centralis (\*) and extending to the margin of the optic disc (arrow). **(B)** Axial balanced steady-state gradient-echo MR image shows a corresponding retinoblastoma (solid arrow) along the temporal aspect of the right globe, extending over the optic disc (dotted arrow). **(C)** Axial contrast-enhanced fat-saturated T1-weighted MR image shows homogeneous avid enhancement within the retinoblastoma (solid arrow) with subtle interruption of the normal enhancement of the choroidoretinal complex at the optic disc (dotted arrow), suspicious for prelaminar invasion.

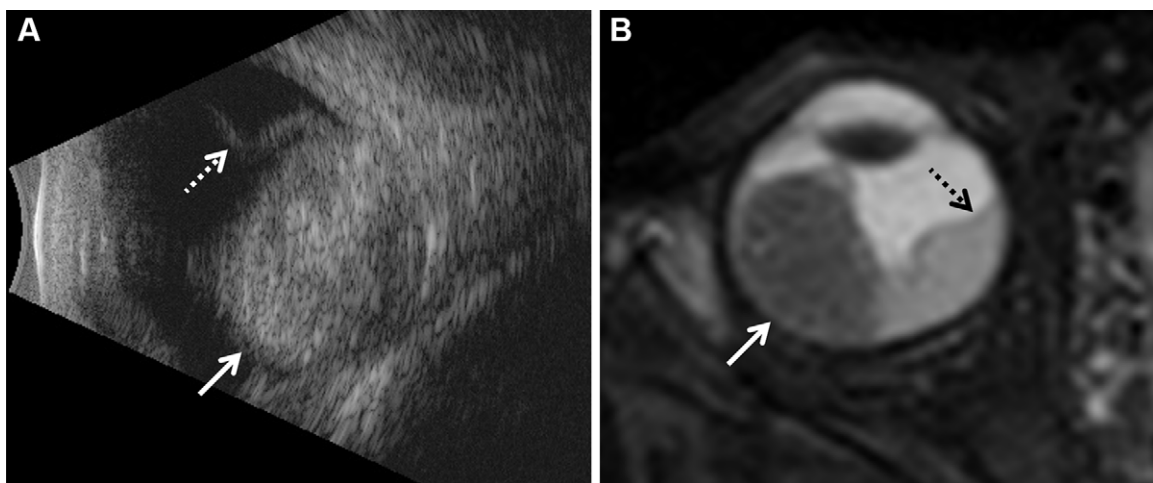


**Figure 11.** Retinoblastoma with retinal detachment (cT2a) involving the right eye in a 23-month-old girl. **(A)** B-mode US image shows an echogenic retinoblastoma (solid arrow) associated with a curvilinear reflective membrane floating in the vitreous, representing retinal detachment (dotted arrow). **(B)** Axial fat-saturated T2-weighted MR image shows a well-defined retinoblastoma (solid arrow) with hypointense signal with extensive detachment of the retina (dotted arrow).

therapy (35). The prevalence of cT2a is estimated to be 10.6%, with a 5-year survival rate of 98% (35,36). At MRI, the detached retina can be seen as a distinct T2-hypointense line focally around the tumor or may show the typical V-shaped appearance in total detachment (Fig 11) (23). MRI has a sensitivity of 50%–89% and specificity of 88%–100% in detection of retinoblastoma-related retinal detachment (23).

### Vitreous and Subretinal Seeding

Growing retinoblastomas may undergo anchorage-independent mutations that promote the detachment and dissemination of tumor into the vitreous cavity and/or subretinal space (1,37). Despite the avascular environment, vitreous and subretinal seeds remain viable and even grow (37). Seeding is a

common cause of treatment failure attributed to the relative avascularity of vitreous and subretinal environments limiting access to chemotherapy (37). Additionally, their small size and diffuse distribution limits control with aggressive local therapy, often necessitating intravitreal chemotherapy (27,28,37).

Fundus photography remains the modality of choice for detection of vitreous seeding as small as 50  $\mu\text{m}$  (38). MRI plays a limited role as seeds are usually near or below the anatomic resolution of thin-section sequences (38). Caution must be exercised because the absence of vitreous seeding at MRI does not rule out its presence (1). When visible, vitreous seeds are seen as small foci of T2 hypointensity on the background of the hyperintense vitreous (Fig 12) (3).

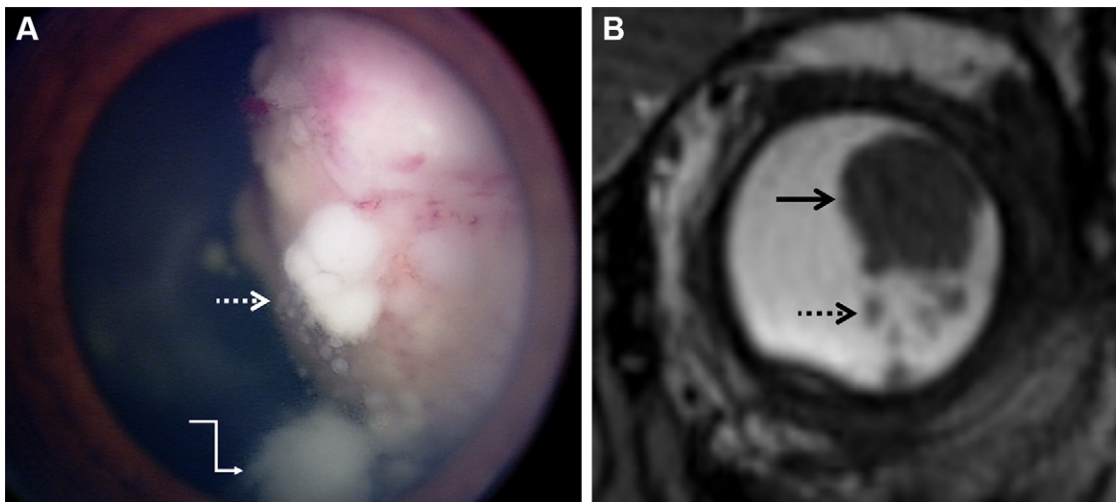


**Figure 12.** Retinoblastoma with vitreous seeds (cT2b) involving the left eye in a 22-month-old girl. **(A)** Wide-field retinal photograph shows retinoblastoma with vitreous seeding, including clouds (bent arrow) and “greasy” pearl-like spheres (dotted arrow) of tumor cells. **(B)** Coronal reconstruction of a balanced steady-state gradient-echo MR image acquired in the axial plane shows an endophytic retinoblastoma (solid arrow) with multiple vitreous seeds (dotted arrow).

### Phthisis or Prephthisis Bulbi

Eyes with retinoblastoma may be smaller than healthy eyes. de Graaf et al (39) found that compared with normal eyes, eyes with retinoblastoma had shorter axial lengths (95% CI: -0.57 mm, -0.16 mm;  $P = .001$ ) and equatorial diameters (95% CI: -1.01 mm, -0.66 mm;  $P < .001$ ) with significantly smaller eye volume (95% CI: -336 mm<sup>3</sup>, -151 mm<sup>3</sup>;  $P < .001$ ). This may be attributed to mechanical restriction of ocular growth by the retinoblastoma (39).

Phthisis bulbi is an uncommon presenting sign of retinoblastoma (0.5–5.3%). Patients usually present between 4 and 14 months of age (40). It is thought to be the end stage of tumor necrosis (due to tumor overgrowth or central retinal artery occlusion) inciting an inflammatory response (40). Phthisis bulbi may represent complete regression of retinoblastoma without residual active tumor. However, continued tumor proliferation in phthisical eyes has been observed (41). The presence of a calcified mass within a phthisical globe must direct attention to retinoblastoma (40). Often, detection of calcification in a shrunken disorganized globe may be difficult. In such cases, the presence of a contralateral retinoblastoma may be a useful guide (40).

### Choroid Invasion

The choroid is a vascular-rich layer between the retina and sclera that caters to the high metabolic need of the photoreceptors (42). Owing to its dense vasculature and peripheral location, choroid invasion increases risk for hematogenous and extraocular spread (1,34). Choroid invasion is encountered in 23%–42% of enucleated retinoblastomas and is referred to as “massive” when the choroidal involvement is more than 3 mm in its largest diameter or when the tumor abuts the inner sclera (20,43).

Massive choroid invasion is associated with an increased risk of metastasis, warranting prompt enucleation and adjuvant systemic chemotherapy (3). In a recent study by Loya et al (44),

no significant difference was found in the all-cause mortality risk in patients with focal (<3 mm) choroid invasion (hazard ratio, 2.69; 95% CI: 0.17, 43.09;  $P = .484$ ). However, massive choroid invasion was associated with a higher risk of all-cause mortality (hazard ratio, 41.29; 95% CI: 4.05, 420.49;  $P = .002$ ) (44). They found that all cancer-related deaths occurred in those with choroid invasion and postlaminar ON invasion (44).

At MRI, the choroid can be identified as a thin avidly enhancing layer, just beneath the nonenhancing sclera (1,20). Discontinuity and thickening of the normal curvilinear choroid may be an imaging marker of choroid invasion (Fig 13) (20). Accurate detection of choroid invasion at MRI is often hampered by the extent of retinal destruction. In scenarios where the entire retinal pigment epithelium is destroyed, distinction between the normal choroidal enhancement and tumor enhancement may be challenging, leading to false-positive interpretations (34).

The sensitivity and specificity of MRI in the detection of choroid invasion is 74% (95% CI: 52%, 88%) and 72% (95% CI: 31%, 94%), respectively (45). Using the 3-mm choroid invasion criterion and the extent to the scleral margin at MRI, Hiasat et al (46) observed an accuracy of 48% (sensitivity, 33%; specificity 97%) and 84% (sensitivity, 53%; specificity, 98%) in the detection of focal and massive choroid invasion, respectively. de Jong et al (47) observed a moderate association between tumor size and massive choroid invasion.

### Anterior Segment Invasion

Retinoblastoma may invade the anterior chamber of the eye across the anterior vitreous face (48). Anterior segment invasion indicates involvement of the ciliary body, lens, iris, and/or cornea and is a high-risk feature for hematogenous spread, warranting enucleation (1,3). The 5-year disease-free survival rate of patients with confirmed anterior segment invasion was found to be 0.9 (95% CI: 0.8, 0.95), with no significant difference in patients with other risk factors with and without

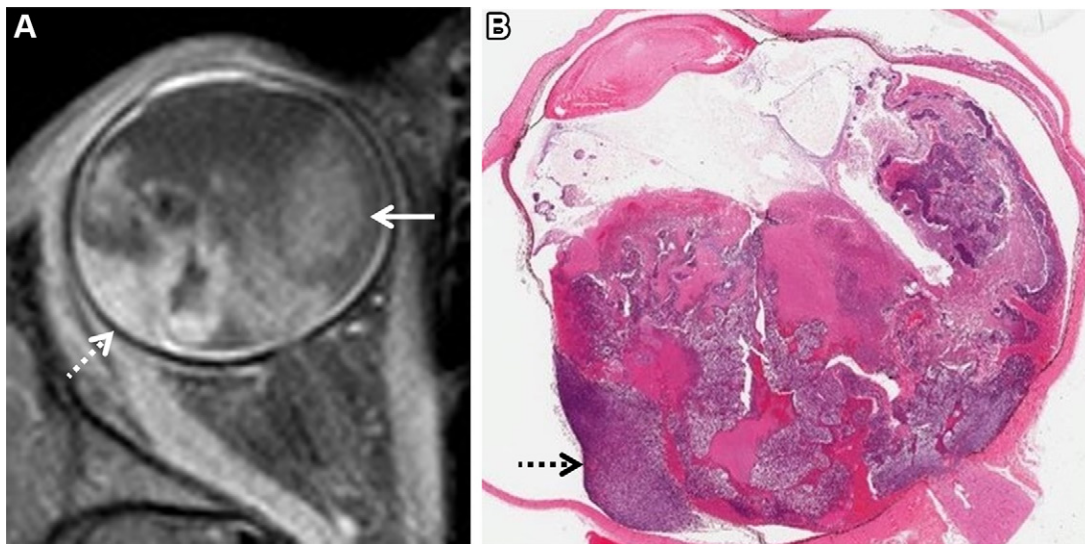


**Figure 13.** Retinoblastoma invading the choroid (cT3b) of the right eye in a 3-year-old girl. **(A)** Axial contrast-enhanced fat-saturated T1-weighted MR image shows a heterogeneously enhancing retinoblastoma (solid arrow). Note the thickening and discontinuity of the normal curvilinear choroidal enhancement (dotted arrow) suggestive of choroidal invasion. **(B)** Low-magnification photomicrograph of a histopathologic specimen obtained after enucleation confirms the choroidal invasion (arrow) >3 mm in its largest dimension; ie, pathologic stage pT3a).

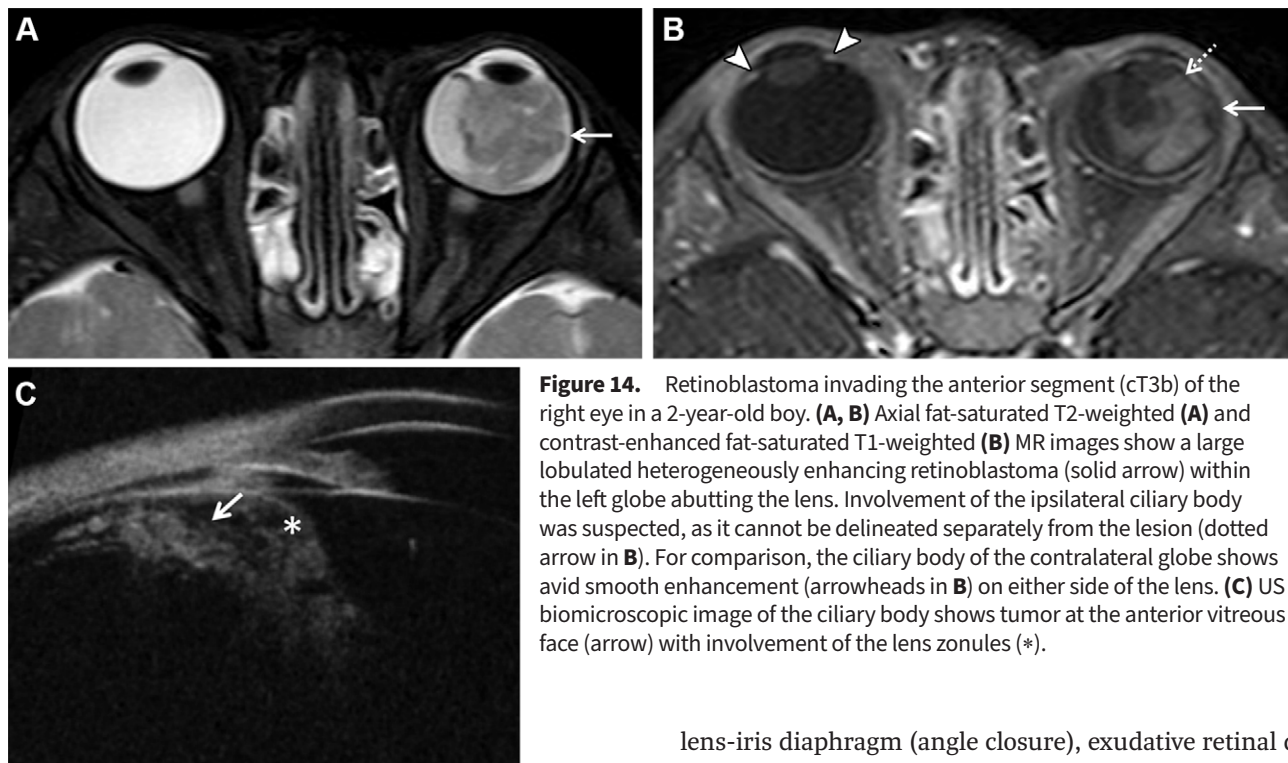


**Figure 14.** Retinoblastoma invading the anterior segment (cT3b) of the right eye in a 2-year-old boy. **(A, B)** Axial fat-saturated T2-weighted **(A)** and contrast-enhanced fat-saturated T1-weighted **(B)** MR images show a large lobulated heterogeneously enhancing retinoblastoma (solid arrow) within the left globe abutting the lens. Involvement of the ipsilateral ciliary body was suspected, as it cannot be delineated separately from the lesion (dotted arrow in **B**). For comparison, the ciliary body of the contralateral globe shows avid smooth enhancement (arrowheads in **B**) on either side of the lens. **(C)** US biomicroscopic image of the ciliary body shows tumor at the anterior vitreous face (arrow) with involvement of the lens zonules (\*).

anterior segment invasion (49). Anterior segment invasion is uncommon and is typically associated with an anteriorly located retinoblastoma (20). Enhancement of the ciliary body or beyond, contiguous with the tumor, should raise suspicion for anterior segment invasion (Fig 14) (20). MRI detection of ciliary body invasion showed a sensitivity of 71%–100% and specificity 65%–100% in a meta-analysis by de Jong et al (45). However, US biomicroscopy has shown better results, with a reported sensitivity and specificity of 80% (95% CI: 44%, 97%) and 95% (95% CI: 83%, 99%), respectively (50).

### Raised Intraocular Pressure

Glaucoma in the context of retinoblastoma (1%–23%) occurs due to neovascularization of the iris, displacement of the

lens-iris diaphragm (angle closure), exudative retinal detachment, tumor seeding of the trabecular meshwork, and uveitis or pseudouveitis with tumor cells and/or inflammatory cells (51). Eyes with an intraocular pressure greater than or equal to 34 mm Hg at the time of diagnosis were 5.91 times more likely to have high-risk features at enucleation compared with those below this value (52). On MR images, signs of increased intraocular pressure include increase in the size of the globe, contour deformity of the globe, and reduced depth of the anterior chamber depth (20).

### Iris Neovascularization

Physiologic leakage of contrast material into the anterior chamber occurs across the blood-aqueous barrier at the root of the iris (53). A negative correlation has been observed between anterior chamber contrast material concentration and the patient's age (between 0 and 8 years), suggesting either a high

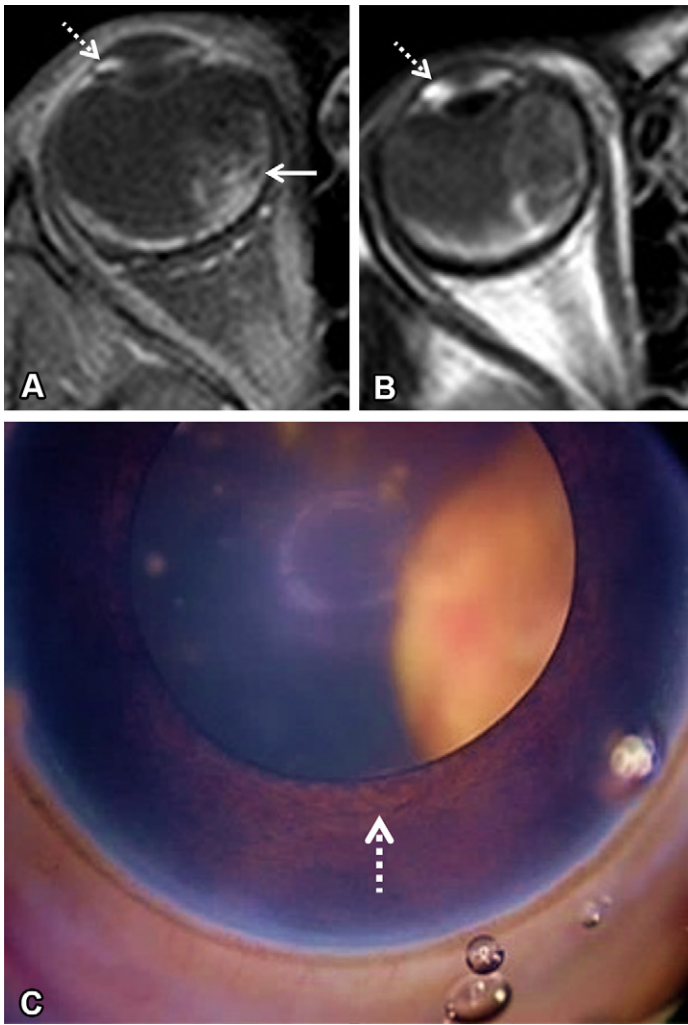


**Figure 15.** Retinoblastoma (cT3c) associated with neovascularization of the iris in the right eye in a 2-year-old boy. **(A)** Axial contrast-enhanced fat-saturated T1-weighted MR image shows a heterogeneously enhancing retinoblastoma (solid arrow) with subtle enhancement within the anterior segment (dotted arrow). **(B)** Axial contrast-enhanced fluid-attenuated inversion-recovery MR image through the orbits, obtained as a part of contrast-enhanced imaging of the brain, shows interval increased enhancement within the anterior segment (arrow). **(C)** Wide-field photograph of the iris shows the neovascularization (arrow).

blood-aqueous barrier permeability or a low efflux capacity of drainage through the Schlemm canal in younger children (53).

While this may be a normal phenomenon in healthy eyes, anterior chamber contrast enhancement in retinoblastoma may indicate a sinister cause (Fig 15). Deike-Hofmann et al (54) hypothesized that neovascularization of the iris may occur due to blockage of the orbital glymphatic pathway (also responsible for anterior chamber drainage) along the lamina cribrosa by an obstructing retinoblastoma. This causes toxin accumulation in the retina leading to vascular endothelial growth factor release promoting neovascularization of the iris. The neovascularized iris is permeable, allowing contrast material seepage into the anterior chamber (54).

Anterior chamber enhancement indicates neovascularization of the iris with a sensitivity of 68%–93% and specificity of

43%–82% (45). A significant correlation exists between degree of anterior chamber enhancement and iris surface–vessel count, tumor volume, and signs of retrolaminar ON invasion at MRI (55). An association has also been noted between abnormal anterior chamber enhancement and elevated intraocular pressure, growth of retinoblastoma beyond the equator, and neovascularization of the iris at histopathologic analysis, as well as histopathologic evidence of ON invasion and/or choroid invasion (56). Abnormal anterior chamber enhancement in patients with retinoblastoma must alert the radiologist and ophthalmologist to the aggressive behavior of the tumor and to the possibility of high-risk features (56).

### **Hyphema and Vitreous Hemorrhage**

Hemorrhagic complications of retinoblastoma are considered high-risk features for metastatic dissemination (14-fold risk compared with that of cT2a) (35). Hyphema (5% of retinoblastoma cases) is thought to occur secondary to neovascularization of the iris. Paracentesis of hyphema in the setting of retinoblastoma is contraindicated due to an increased metastatic risk, making it essential to perform ocular US in children with hyphema when the retina is unexaminable (57). Vitreous hemorrhage is encountered in less than 3% of retinoblastoma cases, which complicates ophthalmoscopic evaluation of retinoblastoma (1,3). On MR images, vitreous hemorrhage demonstrates T1 and T2 shortening (Fig 16) (1).

### **Aseptic Orbital Cellulitis**

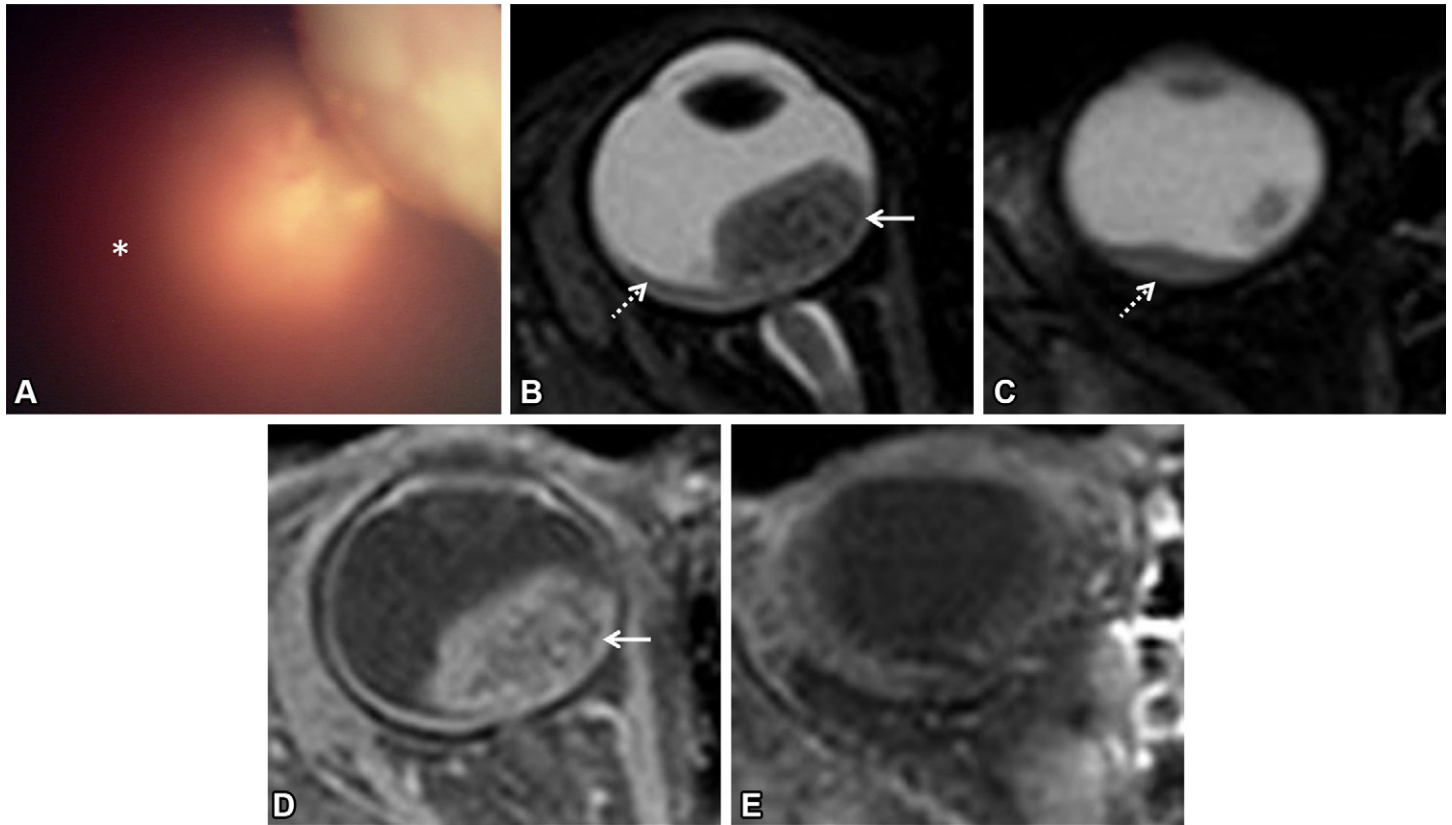
Retinoblastoma-associated orbital cellulitis is a rare (about 5% of retinoblastoma cases) sterile inflammatory response to the tumor undergoing autoinfarction (58). Total retinal detachment is also thought to affect blood flow, contributing to tumor ischemia (58). Soft-tissue swelling, conjunctival chemosis, uveitis, rubeosis iridis, elevated intraocular pressure, and buphthalmos are clinical features of retinoblastoma-associated orbital cellulitis (58).

MRI signs of retinoblastoma-associated orbital cellulitis include a nonenhancing necrotic T2-hypointense tumor with periocular inflammatory changes and lens subluxation (ciliary body necrosis) (Fig 17) (58). Occasionally, contrast enhancement may be seen in the postlaminar ON, secondary to inflammation rather than invasion (58). Enhancement equal to or greater than that of the choroid, which covers the entire width of the lamina cribrosa, and postlaminar ON may suggest inflammation (58). On the other hand, postlaminar ON invasion is usually a triangular region of enhancement, isointense to the tumor enhancement and hypointense to the choroid (58). Jansen et al (58) found that using these enhancement patterns increases specificity of detection of postlaminar ON invasion in patients with retinoblastoma-associated orbital cellulitis from 32% (95% CI: 16%, 52%) to 89% (95% CI: 72%, 98%) (58).

### **Postlaminar ON Invasion**

In contradistinction to prelaminar ON involvement, postlaminar ON invasion has been identified as a high-risk feature for poor prognosis with increased risk of orbital recurrence after enucleation (59). Postlaminar ON invasion carries a 16% risk

**Figure 16.** Retinoblastoma (cT3d) associated with vitreous hemorrhage in the right eye of a 3-year-old boy. **(A)** Wide-field retinal photograph shows a large diffuse tumor, indistinct from a diffuse vitreous bleed (\*). **(B, C)** Sequential craniocaudal axial fat-saturated T2-weighted MR images show a well-defined hypointense retinoblastoma (solid arrow in **B**) with layering of T2-hypointense hemorrhagic products along the medial and inferior aspects of the lesion (dotted arrow in **B** and **C**). A gradient-echo image (not shown) was severely distorted due to susceptibility artifacts from adjacent bony structures. **(D, E)** Sequential craniocaudal axial fat-saturated contrast-enhanced T1-weighted MR images obtained at the same levels as **B** and **C** show enhancement only within the tumor (arrow in **D**).



of metastatic dissemination, with a mortality rate as high as 89% (1,60). With the introduction of ocular salvage and consequent lack of histopathologic examination, accurate detection of postlaminar ON invasion is critical to ensure appropriate treatment. Postlaminar ON invasion is a contraindication to intra-arterial chemotherapy (61). Additionally, detection of postlaminar ON invasion can also guide the surgeon to ensure a disease-free resection margin (62).

MRI is the imaging modality of choice for detecting postlaminar ON invasion. In a retrospective study, MRI outperformed CT, respectively, in terms of sensitivity (60% vs 0%), specificity (95% vs 100%), and accuracy (91% vs 94%), as well as negative (95% vs 94%) and positive predictive values (60% vs not assessed) (63). In patients with a normal caliber of the ON, abnormal contrast enhancement (ie,  $\geq 2$  mm in diameter) in the postlaminar segment has been described as an imaging finding of postlaminar ON invasion (Fig 18) (20). Occasionally, focal enhancement of the central retinal vasculature at the globe-nerve junction may be misinterpreted as postlaminar ON invasion (3). Additionally, patients with increased intraocular pressure might have a posterior bulging of the lamina cribrosa, simulating postlaminar ON invasion (3).

In a meta-analysis, the sensitivity of MRI in detecting postlaminar ON invasion was found to be 59% (95% CI: 37%,

78%) with a specificity of 94% (95% CI: 84%, 98%) (45). Using high-resolution orbit surface coils in a 1.5-T MRI unit, a sensitivity and specificity of 60% and 88.7% has been reported for postlaminar ON invasion (64). Li et al (32) observed that bilateral retinoblastomas (odds ratio: 15.32; 95% CI: 1.63, 143.51), tumor covering the optic disc (odds ratio: 6.43; 95% CI: 1.04, 39.79); and ON enhancement (odds ratio: 8.43; 95% CI: 3.50, 20.31) were significant independent factors for postlaminar ON invasion. Further, T2 isointensity (to that of gray matter) was an independent factor in excluding postlaminar ON invasion (32).

de Jong et al (47) found that for patients with postlaminar ON invasion, the receiver operating characteristic analysis of volume and diameter yielded an area under the curve of 0.77 (95% CI: 0.70, 0.85;  $P < .0001$ ) and 0.78 (95% CI: 0.71, 0.85;  $P < .0001$ ), respectively. Further, for the detection of concomitant postlaminar ON invasion and massive choroid invasion, volume and diameter showed an area under the curve of 0.81 (95% CI: 0.70, 0.91;  $P = .0032$ ) and 0.83 (95% CI: 0.73, 0.93;  $P = .0016$ ), respectively (47). Overall, their study established that both postlaminar ON invasion and massive choroidal invasion showed correlation with tumor size. From a clinical perspective, these size cutoffs may play an important role in estimating the risk of harboring high-risk features, which would be important from a treatment planning perspective. Brisse et al (59)

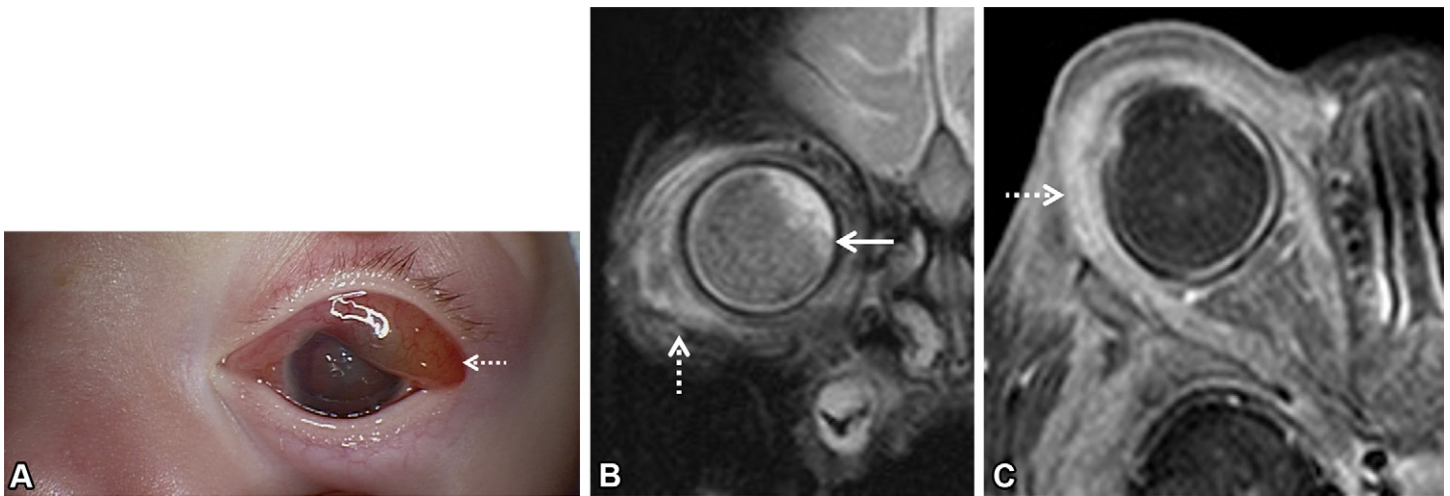
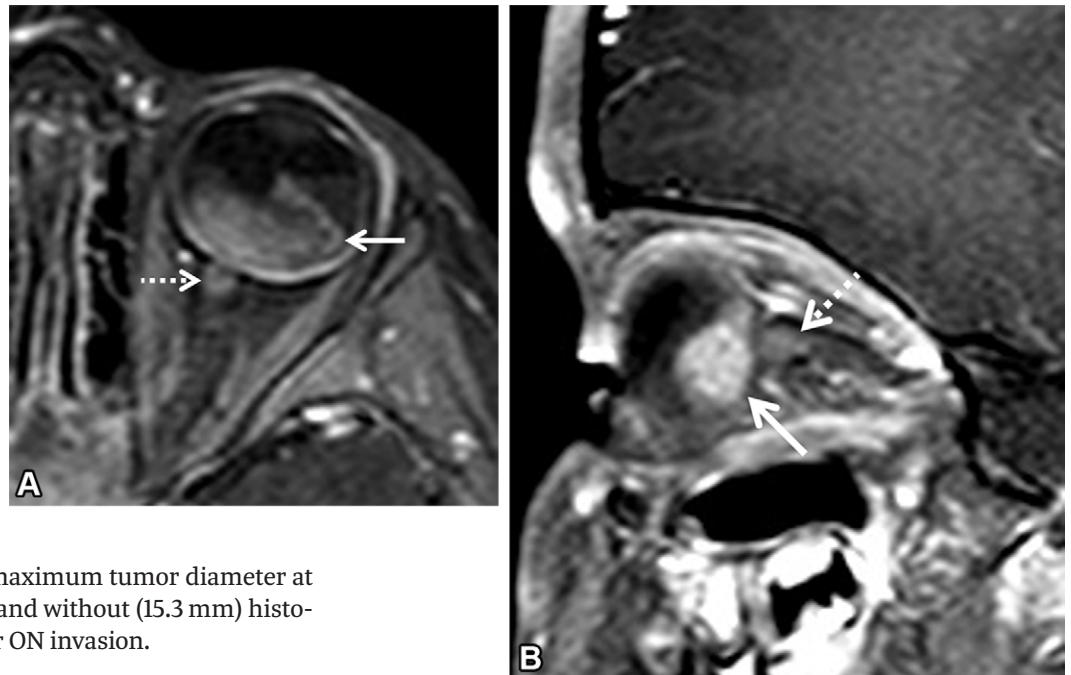


**Figure 17.** Asseptic cellulitis associated with retinoblastoma (stage cT3e) in a 1-year-old girl. **(A)** Clinical photograph shows conjunctival chemosis (arrow). **(B)** Coronal fat-saturated T2-weighted MR image shows a large hypointense retinoblastoma (solid arrow) associated with extensive periocular fat stranding (dotted arrow). **(C)** Axial contrast-enhanced fat-saturated T1-weighted MR image shows no enhancement within the retinoblastoma due to necrosis. Note the extensive inflammatory enhancement in the periocular soft tissues (arrow).

**Figure 18.** Postlaminar ON invasion with retinoblastoma (cT4a) involving the left eye in a 3-year-old girl. Axial **(A)** and oblique sagittal **(B)** contrast-enhanced fat-saturated T1-weighted MR images show heterogeneous enhancement within the retinoblastoma (solid arrow) with contiguous enhancement within the postlaminar ON (dotted arrow), extending for a distance of 3.2 mm (calipers not shown).



found a significant difference in maximum tumor diameter at MRI between eyes with (17.6 mm) and without (15.3 mm) histopathologically proven postlaminar ON invasion.

### Scleral and Extrascleral Invasion

The prevalence of scleral and extrascleral invasion ranges between 3% and 30%, resulting in metastasis and a poor clinical outcome (1,3,6). Cuenca et al (65) found a 5-year survival rate of 77% in patients with scleral and extrascleral invasion. Although massive extension is evident, small focal invasion may be clinically occult, reinforcing the value of MRI (1).

At MRI, scleral invasion can be identified when tumor enhancement extends across the choroid, interrupting the nonenhancing sclera (20). Extrascleral invasion is suspected when tumor enhancement extends into periocular tissues (Fig 19) (1,20). The reported sensitivity and specificity of MRI in the diagnosis of scleral invasion is 88% (95% CI: 20%, 100%) and 99% (95% CI: 86%, 100%) (45). The accuracy of MRI for detecting extrascleral invasion was determined to be 95% (sensitivity, 60%; specificity, 98%) (46).

### Distant and Systemic Metastasis

Extraocular extension of retinoblastoma is an important risk factor for development of distant non-central nervous system metastases, allowing tumoral access to vascular and lymphatic channels (66). Hematogenous spread may also occur in patients with postlaminar ON invasion or choroid invasion (1). Typical systemic metastatic sites include the lungs, liver, and marrow (1) (Fig 20). Hepatic and pulmonary metastases are best evaluated at MRI or CT, while skeletal metastases can be detected at scintigraphy, PET, or MRI with fat-saturated T2-weighted and contrast-enhanced fat-saturated T1-weighted sequences (1). Whole-body MRI can be used in the surveillance for secondary neoplasms in survivors of heritable retinoblastoma. Metastases to the central nervous system are

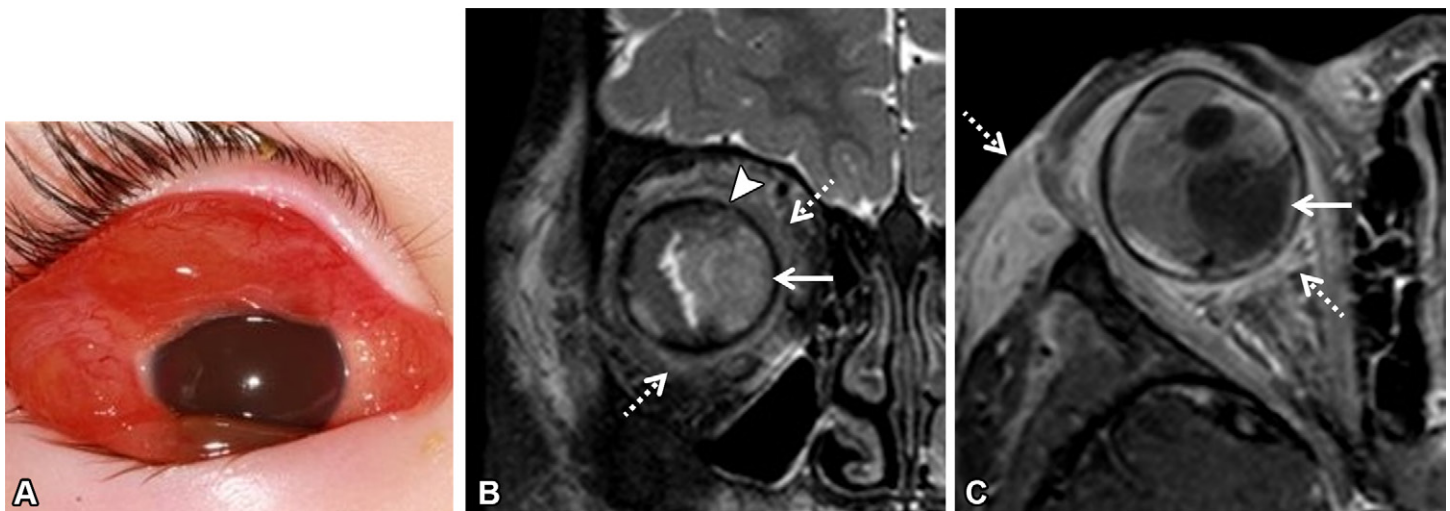


**Figure 19.** Extrascleral extension of retinoblastoma (cT4b) in a 3-year-old boy who presented with severe right-sided proptosis. **(A)** Clinical photograph shows severe conjunctival chemosis. **(B, C)** Coronal fat-saturated T2-weighted **(B)** and axial contrast-enhanced fat-saturated T1-weighted **(C)** MR images show a hypointense nonenhancing retinoblastoma due to necrosis (solid arrow), with a focal breach of the sclera (arrowhead in **B**). Note the enhancing periocular soft-tissue thickening and stranding (dotted arrows).

more common in patients with postlaminar ON invasion, resulting from tumor infiltration into the subarachnoid space around the ON, with subsequent cerebrospinal fluid dissemination (Fig 21) (1,66).

### Heritable Retinoblastoma

The eighth edition of the AJCC staging guidelines for retinoblastoma introduces a new stage group to the system, using H to indicate patients with heritable autosomal dominant susceptibility for retinoblastoma and an increased risk of developing nonocular tumors. Stage H1 includes all patients with bilateral retinoblastoma, trilateral retinoblastoma (retinoblastoma with intracranial central nervous system midline embryonic tumor), or a family history of retinoblastoma, or those with an *RBI* pathogenic variant identified in blood test results. Evaluation of anatomic features specific to H1 disease in all individuals with retinoblastoma or with a risk of heritable retinoblastoma has been recommended (12,20).

### Midline Embryonic Tumors

The neuroectoderm precursor of the pineal gland is prone to develop neoplasms in heritable retinoblastoma (AJCC stage H1), resulting in lesions histologically similar to retinoblastoma (67,68). Suprasellar lesions may occur, arising from ectopic pineal tissue or migrational rudiments of the retina (69). The term *trilateral retinoblastoma* represents bilateral ocular disease with an intracranial midline (pineal or suprasellar) embryonal tumor, with lesions at all four sites called *quadri-lateral retinoblastoma* (68). Pineal lesions account for 75% of all midline embryonal tumors in the context of retinoblastoma (70). The risk of development of pineal lesions is less than 0.5% in unilateral retinoblastomas (68). Approximately 3.2% of all patients with H1 retinoblastoma develop an intracranial midline embryonal lesion, with 2.9% occurring in those with bilateral tumors (70). The median interval between detection of an ocular retinoblastoma (unilateral or bilateral) and an intracranial tumor is 21 months (1).

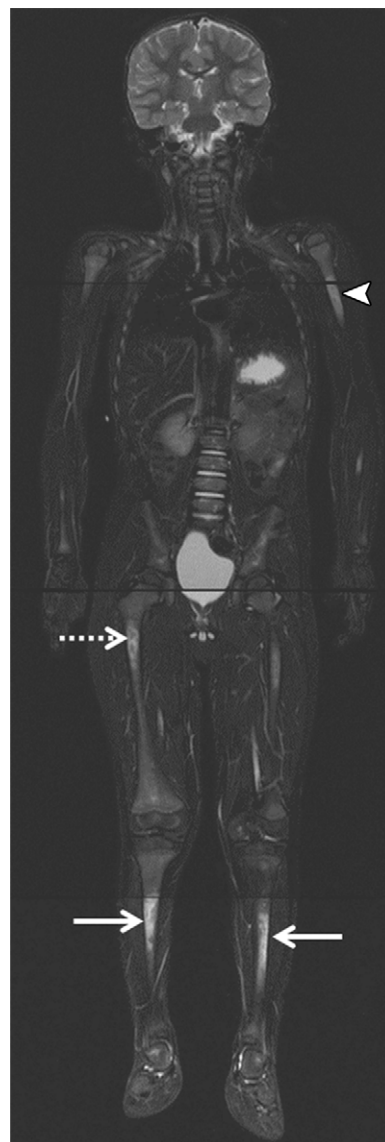


**Figure 20.** Distant metastases in a 4-year-old patient with retinoblastoma (cM1a). Whole-body short tau inversion-recovery screening MR image shows multifocal areas of marrow involvement, particularly in the shafts of the left humerus (arrowhead), right femur (dotted arrow), and tibia on both sides (solid arrows).

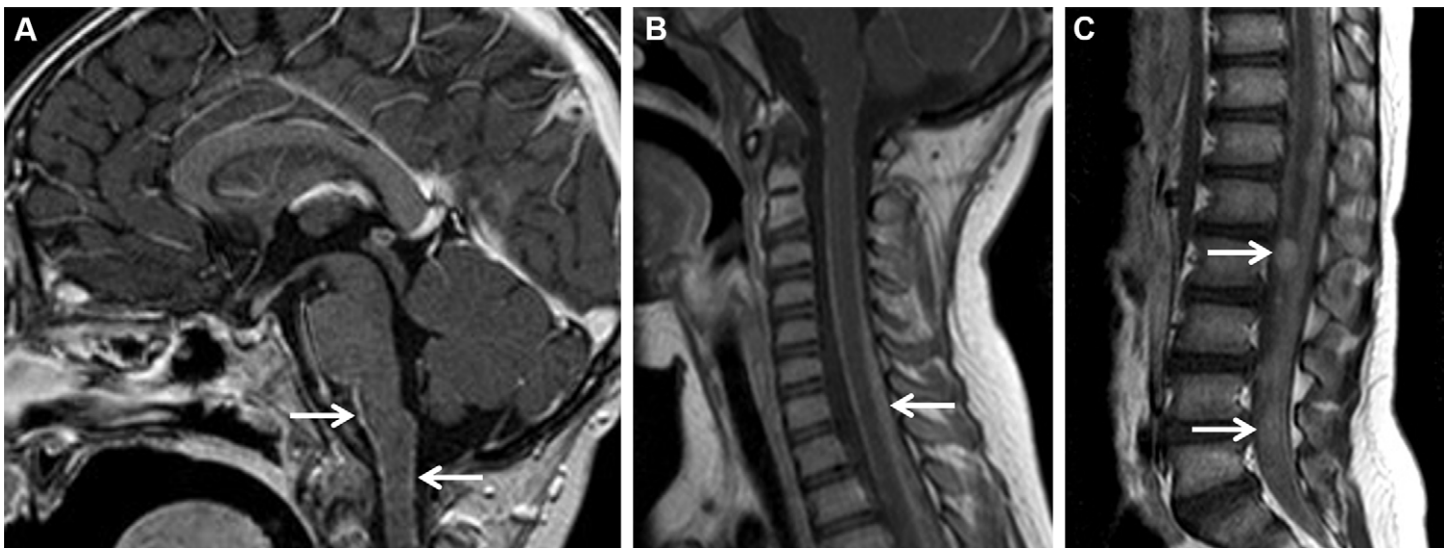


**Figure 21.** Central nervous system metastasis in a 3-year-old girl with retinoblastoma (cM1b). **(A)** Sagittal contrast-enhanced 3D T1-weighted magnetization-prepared rapid gradient-echo (MPRAGE) MR image through the brain shows leptomeningeal enhancement (arrows) along the ventral and dorsal surfaces of the brainstem. **(B, C)** Sagittal contrast-enhanced T1-weighted MR images through the spine show extensive leptomeningeal enhancement along the cervical spine (arrow in **B**), as well as along the conus and cauda equina nerve roots (arrows in **C**).

On MR images, these intracranial lesions demonstrate imaging features similar to those of retinoblastoma (T2 hypointense with restricted diffusion) (Fig 22) (3). Tumors are often solid, but cystic components are not uncommon (68). Rojdan et al (68) found that 42% (6 of 14) of pineal lesions were solid, while the rest were partially or completely cystic. The presence of a cystic pineal lesion in the context of retinoblastoma is an imaging conundrum; benign cysts follow cerebrospinal fluid signal intensity and demonstrate thin (<2 mm) smooth mildly enhancing walls (68). In these cases, some recommend follow-up MRI after 6 months, with no additional follow-up after establishing stability (68). Wall thickening (>2 mm) and nodularity must raise suspicion for a neoplastic cause and prompt earlier follow-up imaging (68). Additional findings including obstructive hydrocephalus and leptomeningeal metastases may be encountered (68).

The overall median survival is 12 months (95% CI: 10 months, 14 months) with a 5-year survival rate of 22% (95% CI: 15%, 29%) (71). The 5-year survival rates of pineal and non-pineal embryonal tumor are 44% (26%–61%) and 57% (30%–77%), respectively, with a drastic improvement after 1995 attributed to better treatment strategies (71).

de Jong et al (72) found that 79% of patients with midline lesions were diagnosed with retinoblastoma before 12 months of age. However, baseline MRI failed to detect pineal lesions in 89% of patients, and an additional MRI examination at 29 months of age detected 53% of asymptomatic pineal lesions. This progressively increased to 72%, 87%, and 92%, with two, three, and four additional MRI examinations, respectively (72). In another study, the lead time to a symptomatic pineal lesion was 1 year (70). de Jong et al (70) suggested half-yearly MRI examinations of the brain starting at 6 months for 3 years, with the advantage of detection of metachronous lesions as well.

A checklist summarizing key MRI findings that impact the staging of retinoblastoma (Table 5) is provided.

## Treatment

Treatment options available for children with retinoblastoma depend on the stage of disease, laterality, and the potential for treatment-related morbidity (Table 6, Fig 23). In addition, for children who are from vulnerable populations, treatment costs and access to various therapeutic modalities are considered. Occasionally, the family's social and cultural beliefs can modify the treatment offered. When the goal of treatment is eye and vision salvage, primary treatment with intravenous and intra-arterial chemotherapy allows tumor consolidation followed by focal therapy with cryotherapy and lasers. Intravitreal and intracameral injections of chemotherapeutic agents may be used to treat tumor seeding.

Recurring or resistant tumor activity is sometimes treated with brachytherapy or external beam radiation therapy and enucleation (4,27,28). External beam radiation therapy is no longer recommended as a first-line treatment of intraocular retinoblastoma due to a risk of developing secondary cancers, particularly in children younger than 1 year of age and those with germline *RBI* mutation (4). When retinoblastoma is diagnosed prenatally, small lesions (cT1a and some eyes with cT1b disease) are treated with focal therapies without initial treatment with chemotherapy. Advanced intraocular retinoblastoma with clinical or radiologic features of cT3 disease is a high-risk feature of systemic dissemination, warranting enucleation rather than a conservative approach. Adjuvant treatment is required additionally if the enucleated eye demonstrates pT3 or pT4 disease features. If cure is considered impossible in cases of extraocular disease and extensive metastasis, palliation with chemotherapy and radiation therapy is considered.

## Conclusion

Retinoblastoma management has seen a paradigm shift toward strategies focused on ocular salvage. However, lesions with high-risk features may still need enucleation. As a result,

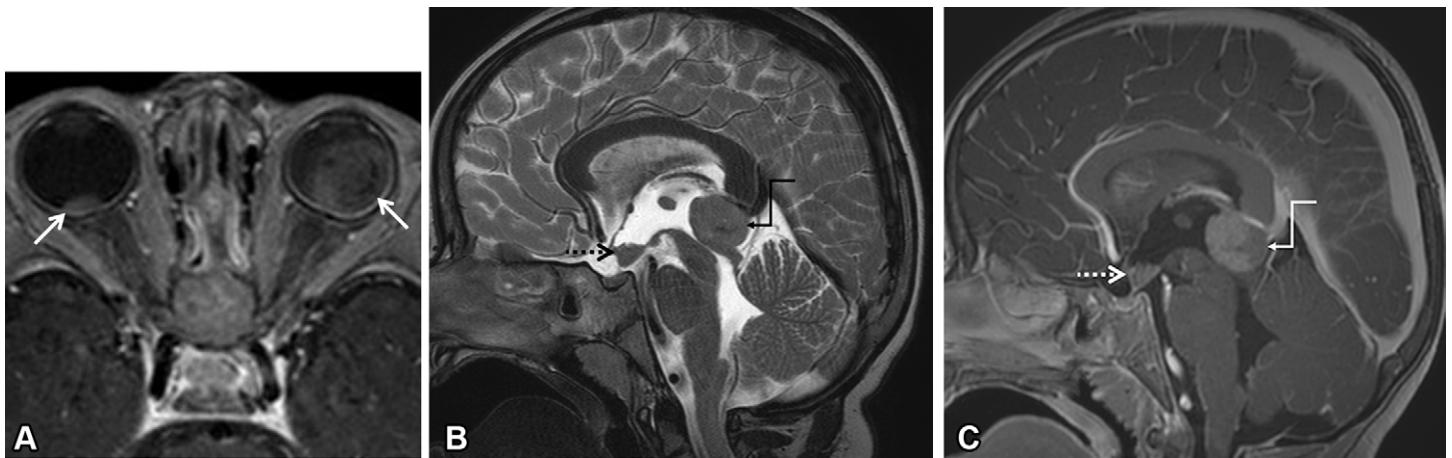


**Figure 22.** Quadrilateral retinoblastoma (H1) in a 10-month-old boy. **(A)** Axial contrast-enhanced T1-weighted MR image of the orbits shows retinoblastomas (arrows) within both globes. **(B, C)** Sagittal T2-weighted **(B)** and contrast-enhanced 3D T1-weighted MPRAGE **(C)** MR images show well-defined hypointense, avidly enhancing mass lesions in the suprasellar (dotted arrow) and pineal (bent arrow) regions, representing midline embryonal tumors.

| Table 5: MRI Checklist for Key Imaging Findings in Retinoblastoma Staging |   |  |
|---|---|--|
| Parameter   | Items to Evaluate   | Relevance  |
| General   | Age<br>Clinical findings<br>Other history   | Early onset associated with hereditary retinoblastoma<br>Leukokoria; ophthalmologic staging<br>Known <i>RBI</i> mutation, family history   |
| Technique   | MRI sequence description  | Adequacy of sequence, motion artifacts   |
| Orbits: tumor   | Laterality<br>Tumor description<br>Location<br>Retinal detachment<br>Seeds<br>Size of the globe<br>Choroidal invasion<br>Vitreous hemorrhage<br>Anterior chamber enhancement<br>Periocular swelling and stranding | Bilateral tumors: common in hereditary retinoblastoma<br>Signal intensity and enhancement<br>Relation to optic disc and fovea<br>Common with exophytic retinoblastoma<br>Best seen with 3D heavily T2-weighted sequences<br>Stage between cT3a and cT3c based on size<br>High-risk feature<br>Upstage to cT3d; may obscure clinical findings<br>Neovascularization of iris, increased risk of ON invasion<br>Aseptic cellulitis, clinical information needed |
| Orbits: advanced retinoblastoma   | Postlaminar ON invasion<br>Scleral breach   | High-risk feature for systemic metastasis<br>Extraocular spread (high-risk feature for systemic metastasis)  |
| Brain   | Midline embryonal tumors<br>Leptomeningeal metastases   | Pineal, sellar, or suprasellar mass associated with retinoblastoma<br>Recommended screening if spinal or distant metastasis is suspected   |
| Time-of-flight MR angiography   | Ophthalmic artery anatomy and variants  | Preplanning access for intra-arterial chemotherapy   |

it is imperative to detect and stage retinoblastomas correctly to ensure appropriate treatment. MRI is the radiologic modality of choice for accurate staging of retinoblastoma. Understanding the limitations and being familiar with the constantly evolving literature form the fundamental basis of detailed and accurate interpretation.

**Author affiliations.**—From the Divisions of Neuroradiology (V.P., P.M., B.E.W., M.M.S., C.P.F.) and Image Guided Therapy (P.M., M.M.S., C.P.F.), Department of Diagnostic Imaging, and Retinoblastoma Program, Department of Ophthalmology and Vision Sciences (K.S., S.K., A.M.), The Hospital for Sick Children (SickKids), University of Toronto, 555 University Ave, Toronto, ON, Canada M5G 1X8; and Department of Pathology and Department of Laboratory Med-

icine and Pediatrics, Cumming School of Medicine, Calgary, Alberta, Canada (M.A.B.). Recipient of a Certificate of Merit award for an education exhibit at the 2022 RSNA Annual Meeting. Received May 8, 2023; revision requested May 30 and received August 7; accepted August 23. **Address correspondence to A.M.** (email: [ashwin.mallipatna@sickkids.ca](mailto:ashwin.mallipatna@sickkids.ca)).

**Disclosures of conflicts of interest.**—**B.E.W.** Radiologic reader for outcome studies for Bayer Healthcare; member of the Board of Directors of the American Society of Pediatric Neuroradiology; shareholder in Munich Medical International; spouse employed by Siemens Healthineers.

**Acknowledgments.**—We acknowledge Dr Samantha Stott (Clinical Fellow, Pediatric Radiology, Department of Diagnostic Imaging, The Hospital for Sick Children [SickKids], University of Toronto, Toronto, Ontario, Canada) and Dr Ria Shetty (Research Assistant, Department of Obstetric Medicine,

| Modality                     | Principle  | Considerations  |
|------------------------------|--|---|
| Intravenous chemotherapy     | Chemotherapeutic agents (vincristine or cyclophosphamide, etoposide, and carboplatin) administered monthly via central or peripheral catheter for 6–9 cycles   | Bilateral disease, postlaminar ON invasion, choroidal invasion, midline embryonal tumors  |
| Intra-arterial chemotherapy  | Supersensitive chemotherapy via the ophthalmic artery (melphalan, topotecan, carboplatin)  | Primary treatment in unilateral tumor (cT1b, cT2, cT3); recurrent or persistent tumor and/or subretinal seeds   |
| Intravitreal chemotherapy    | Melphalan and/or topotecan delivered with an intravitreal injection through the pars plana   | Presence of refractory or recurrent vitreous seeds  |
| Intracameral chemotherapy    | Transcorneal aspiration of aqueous humor followed by injection of equal volume of melphalan or topotecan   | Aqueous seeding or anterior chamber disease in eyes where salvage is considered   |
| Cryotherapy                  | Rapid tumor freezing up to $-87^{\circ}\text{C}$ causing intracellular ice formation, protein denaturation, vascular endothelium damage, tumor infarction; sometimes applied the same day as intravitreal chemotherapy to enhance intraocular drug concentration | Small tumors; foci of subretinal or preretinal seeds  |
| Laser focal therapy          | Laser photocoagulation of tumors and tumor vasculature with 810-nm or 532-nm lasers with a small spot size; mostly used as an adjunct after completion of primary chemotherapy   | Adjunct treatment to active tumors, especially those that are $<3$ mm in diameter and $<2$ mm in thickness  |
| Transpupillary thermotherapy | Application of a gentle heat directly to a tumor, using the 810-nm large-spot laser; indocyanine green may be used to enhance the effects of transpupillary thermotherapy  | Treatment of posterior tumors $<3$ mm in diameter and $<2$ mm in thickness  |
| Proton and photon radiation  | Delivered using stereotactic techniques to minimize off-target radiation   | Extraocular tumor extension; orbital recurrence; positive ON margin following enucleation   |
| Plaque radiation therapy     | Delivered using iodine 125 ( $^{125}\text{I}$ ) or ruthenium 106 ( $\text{Ru}^{106}$ ) surgically placed adjacent to the tumor for a few days  | Second-line therapy of solitary or clustered moderate-sized lesions; chemoresistant lesions with or without vitreous or subretinal seeding; recurrence after intravenous or intra-arterial chemotherapy |
| Enucleation                  | Surgical removal of the eyeball in toto with a long ON stump and placement of an implant   | Advanced intraocular disease, especially in unilateral retinoblastoma; extraocular extension; suspected high-risk features such as postlaminar ON invasion and choroidal invasion; recalcitrant tumors  |

Sources.—References 27, 28.

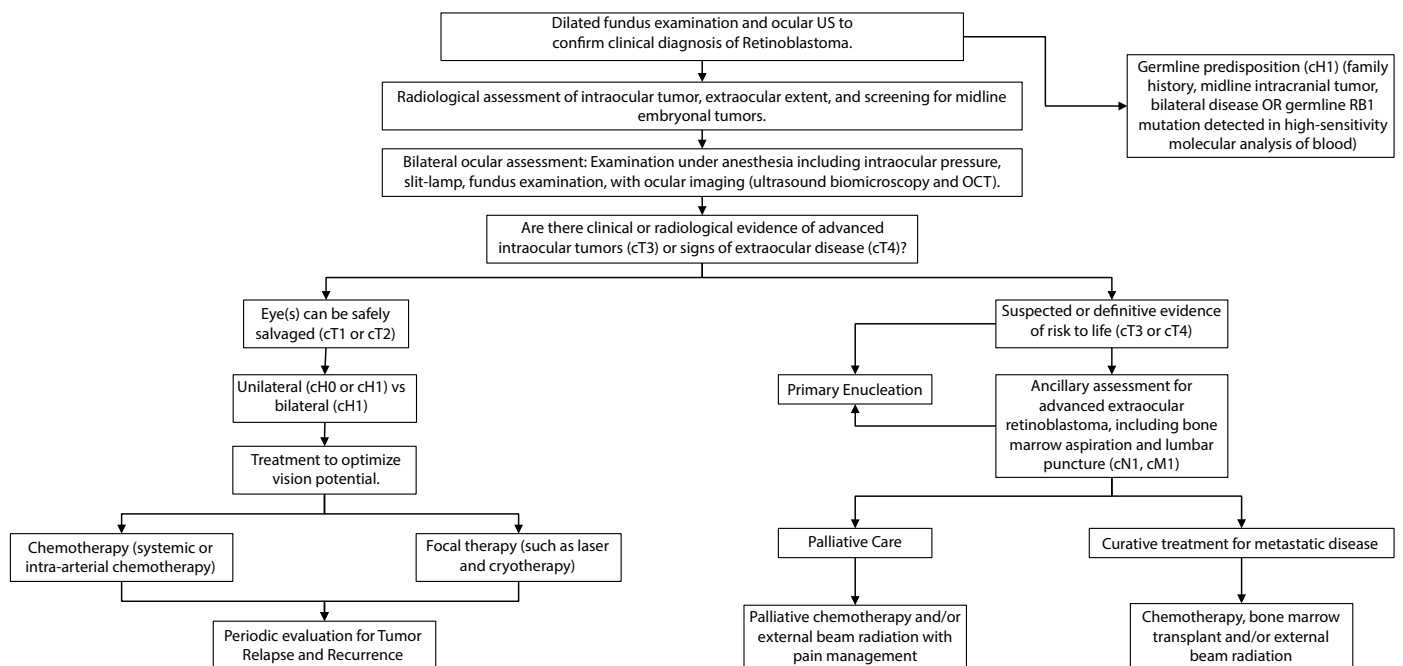


**Figure 23.** Algorithmic approach to workup and treatment in patients with retinoblastoma.

McMaster University, Hamilton, Ontario, Canada) for their contribution in editing the manuscript.

## References

- Rauschecker AM, Patel CV, Yeom KW, et al. High-resolution MR imaging of the orbit in patients with retinoblastoma. *RadioGraphics* 2012;32(5):1307–1326.
- Moez Uddin M, Farooque U, Aziz MZ, et al. Different types of clinical presentations and stages of retinoblastoma among children. *Cureus* 2020;12(9):e10672.
- Silvera VM, Guerin JB, Brinjikji W, Dalvin LA. Retinoblastoma: What the neuroradiologist needs to know. *AJNR Am J Neuroradiol* 2021;42(4):618–626.
- Dimaras H, Corson TW, Cobrinik D, et al. Retinoblastoma. *Nat Rev Dis Primers* 2015;1(1):15021.
- Mallapatna A, Marino M, Singh AD. Genetics of Retinoblastoma. *Asia Pac J Ophthalmol (Phila)* 2016;5(4):260–264.
- Singh L, Kashyap S. Update on pathology of retinoblastoma. *Int J Ophthalmol* 2018;11(12):2011–2016.
- Bremner R, Sage J. Cancer: The origin of human retinoblastoma. *Nature* 2014;514(7522):312–313.
- Jijelava KP, Grossniklaus HE. Diffuse anterior retinoblastoma: A review. *Saudi J Ophthalmol* 2013;27(3):135–139.
- Wippold FJ 2nd, Perry A. Neuroepithelioma for the neuroradiologist: rosettes and pseudorosettes. *AJNR Am J Neuroradiol* 2006;27(3):488–492.
- Novetsky DE, Abramson DH, Kim JW, Dunkel IJ. Published international classification of retinoblastoma (ICRB) definitions contain inconsistencies: an analysis of impact. *Ophthalmic Genet* 2009;30(1):40–44.
- Tomar AS, Finger PT, Gallie B, et al. A Multicenter, International Collaborative Study for American Joint Committee on Cancer Staging of Retinoblastoma: Part II: Treatment Success and Globe Salvage. *Ophthalmology* 2020;127(12):1733–1746 [Published correction appears in *Ophthalmology* 2021;128(8):1245.].
- Mallapatna A, Gallie BL, Chévez-Barríos P, et al. Retinoblastoma. In: Amin MB, Edge SB, Greene FL, eds. *AJCC Cancer Staging Manual*. 8th ed. New York, NY: Springer, 2017; 819–831.
- Dimaras H, Corson TW. Retinoblastoma, the visible CNS tumor: A review. *J Neurosci Res* 2019;97(1):29–44.
- Nadiarnykh O, McNeill-Badalova NA, Gaillard MC, et al. Optical coherence tomography (OCT) to image active and inactive retinoblastomas as well as retinomas. *Acta Ophthalmol* 2020;98(2):158–165.
- Rootman DB, Gonzalez E, Mallapatna A, et al. Hand-held high-resolution spectral domain optical coherence tomography in retinoblastoma: clinical and morphologic considerations. *Br J Ophthalmol* 2013;97(1):59–65.
- Mallapatna A, Vinekar A, Jayadev C, et al. The use of handheld spectral domain optical coherence tomography in pediatric ophthalmology practice: Our experience of 975 infants and children. *Indian J Ophthalmol* 2015;63(7):586–593.
- Nadiarnykh O, Davidoiu V, Gräfe MGO, Bosscha M, Moll AC, de Boer JF. Phase-based OCT angiography in diagnostic imaging of pediatric retinoblastoma patients: abnormal blood vessels in post-treatment regression patterns. *Biomed Opt Express* 2019;10(5):2213–2226.
- Bonanomi MTBC, Saito OC, de Lima PP, Bonanomi RC, Chammas MC. Blood flow in monocular retinoblastoma assessed by Color Doppler and correlations with high-risk pathologic features. *Invest Ophthalmol Vis Sci* 2018;59(13):5441–5446.
- Finger PT, Khoobehi A, Ponce-Contreras MR, Rocca DD, Garcia JP Jr. Three dimensional ultrasound of retinoblastoma: initial experience. *Br J Ophthalmol* 2002;86(10):1136–1138.
- de Graaf P, Göricke S, Rodjan F, et al. Guidelines for imaging retinoblastoma: imaging principles and MRI standardization. *Pediatr Radiol* 2012;42(1):2–14.
- Rodjan F, de Graaf P, van der Valk P, et al. Detection of calcifications in retinoblastoma using gradient-echo MR imaging sequences: comparative study between in vivo MR imaging and ex vivo high-resolution CT. *AJNR Am J Neuroradiol* 2015;36(2):355–360.
- Galluzzi P, Hadjistilianou T, Cerase A, De Francesco S, Toti P, Venturi C. Is CT still useful in the study protocol of retinoblastoma? *AJNR Am J Neuroradiol* 2009;30(9):1760–1765.
- de Jong MC, de Graaf P, Brisse HJ, et al. The potential of 3T high-resolution magnetic resonance imaging for diagnosis, staging, and follow-up of retinoblastoma. *Surv Ophthalmol* 2015;60(4):346–355.
- Abdel Razek AAK, Elkhamary S, Al-Mesfer S, Alkatan HM. Correlation of apparent diffusion coefficient at 3T with prognostic parameters of retinoblastoma. *AJNR Am J Neuroradiol* 2012;33(5):944–948.
- Habib YS, Youssef AA, AlKiki HA, Ghareeb HT, ElZomor HE. High resolution MR imaging guidelines in retinoblastoma: Prospective study correlated with histopathological results. *Egypt J Radiol Nucl Med* 2020;51(1):28.
- Shields CL, Santos MC, Diniz W, et al. Thermotherapy for retinoblastoma. *Arch Ophthalmol* 1999;117(7):885–893.
- Ancona-Lezama D, Dalvin LA, Shields CL. Modern treatment of retinoblastoma: A 2020 review. *Indian J Ophthalmol* 2020;68(11):2356–2365.
- Chawla B, Jain A, Azad R. Conservative treatment modalities in retinoblastoma. *Indian J Ophthalmol* 2013;61(9):479–485.
- Tomar AS, Finger PT, Gallie B, et al. High-risk Pathologic Features Based on Presenting Findings in Advanced Intraocular Retinoblastoma: A Multicenter, International Data-Sharing American Joint Committee on Cancer Study. *Ophthalmology* 2022;129(8):923–932.
- Soliman SE, VandenHoven C, Mackeen LD, Gallie BL. Vision and visual potential for perifoveal retinoblastoma after optical coherence tomographic-guided sequential laser photocoagulation. *Br J Ophthalmol* 2019;103(6):753–760.
- King BA, Parra C, Li Y, et al. Spatiotemporal patterns of tumor occurrence in children with intraocular retinoblastoma. *PLoS One* 2015;10(7):e0132932.
- Li Z, Guo J, Xu X, Wang Y, Mukherji SK, Xian J. Diagnosis of postlaminar optic nerve invasion in retinoblastoma with MRI features. *J Magn Reson Imaging* 2020;51(4):1045–1052.
- Shields CL, Shields JA, Baez K, Cater JR, De Potter P. Optic nerve invasion of retinoblastoma. Metastatic potential and clinical risk factors. *Cancer* 1994;73(3):692–698.
- de Graaf P, Barkhof F, Moll AC, et al. Retinoblastoma: MR imaging parameters in detection of tumor extent. *Radiology* 2005;235(1):197–207.
- El Hamichi S, Acon D, Kon Graversen V, Gold AS, Berrocal AM, Murray TG. Persistent retinal detachment in retinoblastoma: The challenges. *J Ophthalmol* 2020;2020:1486757.
- Tomar AS, Finger PT, Gallie B, et al. Metastatic Death Based on Presenting Features and Treatment for Advanced Intraocular Retinoblastoma: A Multicenter Registry-Based Study. *Ophthalmology* 2022;129(8):933–945.
- Tomar AS, Finger PT, Gallie B, et al. Retinoblastoma seeds: impact on American Joint Committee on Cancer clinical staging. *Br J Ophthalmol* 2023;107(1):127–132.
- Khurana A, Eisenhut CA, Wan W, et al. Comparison of the diagnostic value of MR imaging and ophthalmoscopy for the staging of retinoblastoma. *Eur Radiol* 2013;23(5):1271–1280.
- de Graaf P, Knol DL, Moll AC, Imhof SM, Schouten-van Meeteren AY, Castelljns JA. Eye size in retinoblastoma: MR imaging measurements in normal and affected eyes. *Radiology* 2007;244(1):273–280.
- Kashyap S, Meel R, Pushker N, et al. Phthisis bulbi in retinoblastoma. *Clin Exp Ophthalmol* 2011;39(2):105–110.
- Gallie BL, Phillips RA, Ellsworth RM, Abramson DH. Significance of retinoma and phthisis bulbi for retinoblastoma. *Ophthalmology* 1982;89(12):1393–1399.
- Summers JA. The choroid as a sclera growth regulator. *Exp Eye Res* 2013;114:120–127.
- Sastre X, Chantada GL, Doz F, et al. Proceedings of the consensus meetings from the International Retinoblastoma Staging Working Group on the pathology guidelines for the examination of enucleated eyes and evaluation of prognostic risk factors in retinoblastoma. *Arch Pathol Lab Med* 2009;133(8):1199–1202.
- Loya A, Ayaz T, Gombos DS, Weng CY. Association of choroidal invasion with retinoblastoma survival rates. *J AAPOS* 2023;27(1):32.e1–32.e8.
- de Jong MC, de Graaf P, Noij DP, et al. Diagnostic performance of magnetic resonance imaging and computed tomography for advanced retinoblastoma: a systematic review and meta-analysis. *Ophthalmology* 2014;121(5):1109–1118.
- Hiasat JG, Saleh A, Al-Hussaini M, et al. The predictive value of magnetic resonance imaging of retinoblastoma for the likelihood of high-risk pathologic features. *Eur J Ophthalmol* 2019;29(2):262–268.
- de Jong MC, van der Meer FJ, Göricke SL, et al. Diagnostic Accuracy of Intraocular Tumor Size Measured with MR Imaging in the Prediction of Postlaminar Optic Nerve Invasion and Massive Choroidal Invasion of Retinoblastoma. *Radiology* 2016;279(3):817–826.
- Moulin AP, Gaillard M-C, Balmer A, Munier FL. Ultrasound biomicroscopy evaluation of anterior extension in retinoblastoma: a clinicopathological study. *Br J Ophthalmol* 2012;96(3):337–340.
- Baroni LV, Sampor C, Fandiño A, et al. Anterior segment invasion in retinoblastoma: is it a risk factor for extraocular relapse? *J Pediatr Hematol Oncol* 2014;36(8):e509–e512.
- Chawla B, Bhaskaran K, Dada T, Bajaj MS, Kashyap S, Shende D. Evaluation of the role of ultrasound biomicroscopy in advanced retinoblastoma: A prospective study on Asian Indian children. *Ophthalmic Genet* 2020;41(2):125–130.
- de Leon JM, Walton DS, Latina MA, Mercado GV. Glaucoma in retinoblastoma. *Semin Ophthalmol* 2005;20(4):217–222.

52. Kim ME, Shah S, Zolfaghari E, et al. An intraocular pressure predictive of high-risk histopathologic features in Group E Retinoblastoma Eyes. *Int Ophthalmol Clin* 2019;59(2):77–86.
53. Deike-Hofmann K, von Lampe P, Schlemmer H-P, et al. The anterior eye chamber: entry of the natural excretion pathway of gadolinium contrast agents? *Eur Radiol* 2020;30(8):4633–4640.
54. Deike-Hofmann K, von Lampe P, Eerikainen M, et al. Anterior chamber enhancement predicts optic nerve infiltration in retinoblastoma. *Eur Radiol* 2022;32(11):7354–7364.
55. de Graaf P, van der Valk P, Moll AC, et al. Contrast-enhancement of the anterior eye segment in patients with retinoblastoma: correlation between clinical, MR imaging, and histopathologic findings. *AJNR Am J Neuroradiol* 2010;31(2):237–245.
56. Galluzzi P, Cerase A, Hadjistilianou T, et al. Retinoblastoma: Abnormal gadolinium enhancement of anterior segment of eyes at MR imaging with clinical and histopathologic correlation. *Radiology* 2003;228(3):683–690.
57. Zafar SN, Zaheer N, Khan MA. Retinoblastoma presenting as total hypHEMA: Three year follow-up. *Saudi J Ophthalmol* 2017;31(4):272–274.
58. Jansen RW, van der Heide S, Cardoen L, et al. Magnetic resonance imaging can reliably differentiate optic nerve inflammation from tumor invasion in retinoblastoma with Orbital cellulitis. *Ophthalmology* 2022;129(11):1275–1286.
59. Brisse HJ, de Graaf P, Galluzzi P, et al. Assessment of early-stage optic nerve invasion in retinoblastoma using high-resolution 1.5 Tesla MRI with surface coils: a multicentre, prospective accuracy study with histopathological correlation. *Eur Radiol* 2015;25(5):1443–1452.
60. Berry JL, Zolfaghari E, Chen A, Murphree AL, Jubran R, Kim JW. Optic Nerve Obscuration in Retinoblastoma: A Risk Factor for Optic Nerve Invasion? *Ocul Oncol Pathol* 2017;3(4):283–291.
61. Manjandavida FP, Stathopoulos C, Zhang J, Honavar SG, Shields CL. Intra-arterial chemotherapy in retinoblastoma: A paradigm change. *Indian J Ophthalmol* 2019;67(6):740–754.
62. Cho SJ, Kim JH, Baik SH, Sunwoo L, Bae YJ, Choi BS. Diagnostic performance of MRI of post-laminar optic nerve invasion detection in retinoblastoma: A systematic review and meta-analysis. *Neuroradiology* 2021;63(4):499–509.
63. Brisse HJ, Guesmi M, Aerts I, et al. Relevance of CT and MRI in retinoblastoma for the diagnosis of postlaminar invasion with normal-size optic nerve: a retrospective study of 150 patients with histological comparison. *Pediatr Radiol* 2007;37(7):649–656.
64. Sirin S, Schlamann M, Metz KA, et al. High-resolution MRI using orbit surface coils for the evaluation of metastatic risk factors in 143 children with retinoblastoma: Part 1—MRI vs. histopathology. *Neuroradiology* 2015;57(8):805–814.
65. Cuenca A, Giron F, Castro D, et al. Microscopic scleral invasion in retinoblastoma: clinicopathological features and outcome. *Arch Ophthalmol* 2009;127(8):1006–1010.
66. Gündüz K, Müftüoğlu O, Günalp I, Unal E, Taçyıldız N. Metastatic retinoblastoma clinical features, treatment, and prognosis. *Ophthalmology* 2006;113(9):1558–1566.
67. Gottumukkala RV, Gee MS, Hampilos PJ, Greer MC. Current and emerging roles of whole-body MRI in evaluation of pediatric cancer patients. *RadioGraphics* 2019;39(2):516–534.
68. Rodjan F, de Graaf P, Brisse HJ, et al. Trilateral retinoblastoma: neuroimaging characteristics and value of routine brain screening on admission. *J Neurooncol* 2012;109(3):535–544.
69. Skulski M, Egelhoff JC, Kollias SS, Mazewski C, Ball WS Jr. Trilateral retinoblastoma with suprasellar involvement. *Neuroradiology* 1997;39(1):41–43.
70. de Jong MC, Kors WA, Moll AC, et al. Screening for Pineal Trilateral Retinoblastoma Revisited: A Meta-analysis. *Ophthalmology* 2020;127(5):601–607.
71. de Jong MC, Kors WA, de Graaf P, Castelijns JA, Kivelä T, Moll AC. Trilateral retinoblastoma: a systematic review and meta-analysis. *Lancet Oncol* 2014;15(10):1157–1167.
72. de Jong MC, Shaikh F, Gallie B, et al. Asynchronous pineoblastoma is more likely after early diagnosis of retinoblastoma: a meta-analysis. *Acta Ophthalmol* 2022;100(1):e47–e52.



# Erratum for: Diagnostic Imaging for Retinoblastoma Cancer Staging: Guide for Providing Essential Insights for Ophthalmologists and Oncologists

April 2024 • Volume 44 • Number 4

**Originally published in:**

<https://doi.org/10.1148/rg.230125>

Diagnostic Imaging for Retinoblastoma Cancer Staging: Guide for Providing Essential Insights for Ophthalmologists and Oncologists

Vivek Pai, Prakash Muthusami, Birgit Ertl-Wagner, Manohar M. Shroff, Carmen Parra-Fariñas, Kanchan Sainani, Stephanie Kletke, Marie-Anne Brundler, Ashwin Mallipatna

**Erratum in:**

<https://doi.org/10.1148/rg.249003>

In the article text, Table 1, and the legend for Figure 22, the stage **HI** now appears correctly.